

RECEIVED: December 24, 2022

REVISED: January 15, 2024

ACCEPTED: March 11, 2024

PUBLISHED: April 10, 2024

$B_s \rightarrow \mu^+ \mu^-$ in a two-Higgs-doublet model with flavour-changing up-type Yukawa couplings

Martin S. Lang  and Ulrich Nierste 

*Institute for Theoretical Particle Physics, Karlsruhe Institute of Technology (KIT),
Wolfgang-Gaede-Str. 1, D-76131 Karlsruhe, Germany*

E-mail: m.lang@kit.edu, ulrich.nierste@kit.edu

ABSTRACT: We present a Two-Higgs-Doublet Model in which the structure of the quark Yukawa matrices is governed by three spurions breaking the flavour symmetries of the quark Yukawa sector. The model naturally suppresses flavour-changing neutral current (FCNC) amplitudes in the down-type sector, but permits sizable FCNC couplings in the up sector. We calculate the branching ratio of $B_s \rightarrow \mu^+ \mu^-$ to leading and next-to-leading order of QCD for the case with FCNC couplings of the heavy neutral Higgs bosons to up-type quarks and verify that all counterterms follow the pattern dictated by the spurion expansion of the Yukawa matrices. We find correlations between $B_s \rightarrow \mu^+ \mu^-$, $b \rightarrow s \gamma$, and the Higgs masses. The $B_s - \bar{B}_s$ mixing amplitude is naturally suppressed in the model but can probe a portion of the parameter space with very heavy Higgs bosons.

KEYWORDS: Bottom Quarks, Multi-Higgs Models, Rare Decays, Specific BSM Phenomenology

ARXIV EPRINT: [2212.11086](https://arxiv.org/abs/2212.11086)

Contents

1	Introduction	1
2	2HDM with suppressed down-type FCNC couplings	2
2.1	General Yukawa sector	2
2.2	Spurion expansion	5
3	The decay $B_s \rightarrow \mu^+ \mu^-$	8
4	Computational setup	9
5	The decay $B_s \rightarrow \mu^+ \mu^-$ in the two-Higgs-doublet model of type-II	10
6	Additional contributions in a model with flavour-changing neutral Yukawa couplings	14
6.1	Pseudoscalar Wilson coefficient C_P	15
6.2	Scalar Wilson coefficient C_S	18
7	Phenomenology	18
7.1	Constraints from $b \rightarrow s\gamma$ decays	19
7.2	Higgs searches	20
7.3	$B_s - \bar{B}_s$ mixing	22
8	Summary	24

1 Introduction

Two-Higgs-Doublet models (2HDMs) [1, 2] are popular extensions of the Standard Model (SM) due to their relative simplicity, involving no additional fields apart from a second Higgs doublet. Moreover, a strong motivation to study 2HDMs also comes from theories in which a second Higgs doublet is required due to symmetry arguments, e.g. axion models in the context of the strong CP puzzle [3–5] or minimal supersymmetry [6]. 2HDMs differ in the structure of Higgs-fermion Yukawa couplings. The historically most favoured variants are the so-called type-I and type-II 2HDM in which both up-type and down-type quarks only couple to one of the two Higgs doublets. In these types of 2HDMs, flavour-changing neutral current processes (FCNC) such as the decay $B_s \rightarrow \mu^+ \mu^-$ are loop-suppressed and therefore small masses of the additional Higgs bosons are in principle possible, an appealing feature in the time of early LHC searches. The generic 2HDM (also dubbed “type-III”), with most general Yukawa matrices, exhibits, however, a much richer phenomenology [7–9] in which flavour-changing neutral Higgs-boson couplings are possible, in case up-type or down-type quarks couple to more than one Higgs doublet. The generic 2HDM suffers from a low level of predictivity caused by its large number of parameters and moreover requires that FCNC couplings in the down-type sector are tuned to small values in an ad-hoc way to comply with the many experimental constraints from $s \rightarrow d$, $b \rightarrow s$, and $b \rightarrow d$ FCNC processes. Yet the economic 2HDM of type I and II cannot address current anomalies in rare bottom quark decays, for instance data favour an excess of $\mathcal{B}(B \rightarrow D\tau\nu)/\mathcal{B}(B \rightarrow D\mu\nu)$ over its SM prediction [10–21] and this

cannot be explained in these models. Also to address the observed deficit in $b \rightarrow s\mu^+\mu^-$ for low values of the lepton-pair invariant mass one resorts to the generic 2HDM [9].

In this paper, we propose a three-spurion 2HDM, a 2HDM which is more general than the popular type-I and type-II models (which it contains as limiting cases) but more constrained than the generic 2HDM. A process on which our model has characteristic imprints is $B_s \rightarrow \mu^+\mu^-$, which we study in detail in this paper, including the calculation of two-loop QCD corrections. The model under consideration will feature flavour-changing up-type Yukawa couplings of the additional heavy neutral Higgs bosons, most notably a charm-top transition which may eliminate the Cabibbo-Kobayashi-Maskawa (CKM) suppression in $b \rightarrow s$ transitions that is present in both the SM and the 2HDM type-II models.

The outline of the paper is as follows: the Yukawa and Higgs sectors of the three-spurion 2HDM are presented in section 2, with particular emphasis on some peculiarities of this specific model. In section 3, we will introduce the effective operators contributing to the low-energy weak $B_s \rightarrow \mu^+\mu^-$ decay, while section 4 is dedicated to a short description of the computational setup used for the evaluation of Feynman diagrams. The limiting case of the type-II 2HDM is discussed in section 5, with the additional contributions from flavour-changing neutral-Higgs Yukawa couplings being presented in section 6. Finally, we will discuss the phenomenology of such models in section 7 and summarize in section 8.

2 2HDM with suppressed down-type FCNC couplings

In this section we introduce the so-called *three-spurion 2HDM*, which allows for significant flavour-changing Yukawa couplings in the up-type quark sector, while the ones in the down-type quark sector are naturally suppressed.

2.1 General Yukawa sector

Our starting point, the quark Yukawa Lagrangian of the general (“type III”) 2HDM, reads

$$\begin{aligned} L_Y &= -\bar{Q}'_f \left[\bar{Y}_{fi}^d H_d + \bar{\epsilon}_{fi}^d H_u \right] d'_{iR} - \bar{Q}'_f \left[\bar{Y}_{fi}^u \epsilon H_u^* + \bar{\epsilon}_{fi}^u \epsilon H_d^* \right] u'_{iR} + h.c. \\ &\equiv -\bar{Q}'_f \left[\bar{Y}^d H_d + \bar{\epsilon}^d H_u \right] d'_R - \bar{Q}'_f \left[\bar{Y}^u \epsilon H_u^* + \bar{\epsilon}^u \epsilon H_d^* \right] u'_R + h.c. \end{aligned} \quad (2.1)$$

with four general complex 3×3 matrices $\bar{Y}^{u,d}$ and $\bar{\epsilon}^{u,d}$ as well as

$$H_{u,d} = \begin{pmatrix} H_{u,d}^+ \\ H_{u,d}^0 \end{pmatrix}, \quad \epsilon H_{u,d}^* = \begin{pmatrix} H_{u,d}^{0*} \\ -H_{u,d}^- \end{pmatrix}, \quad (2.2)$$

$$\text{and } Q'_f = \begin{pmatrix} u'_{fL} \\ d'_{fL} \end{pmatrix}. \quad (2.3)$$

The subscripts $f, i = 1, 2, 3$ label the generations, e.g. $u'_{3L} = t'_L$. The notation of eq. (2.1) follows ref. [8], except that our H_d corresponds to $-\epsilon H_d^*$ of that paper. The vacuum expectation values (vevs) and related quantities are

$$\begin{aligned} \langle H_u^0 \rangle &= v_u = v \sin \beta, & \langle H_d^0 \rangle &= v_d = v \cos \beta, \\ \tan \beta &:= \frac{v_u}{v_d}, & v &:= \sqrt{v_u^2 + v_d^2} = 174 \text{ GeV}. \end{aligned} \quad (2.4)$$

The quark mass matrices are

$$M^d = \bar{Y}^d v \cos \beta + \bar{\epsilon}^d v \sin \beta, \quad M^u = \bar{Y}^u v \sin \beta + \bar{\epsilon}^u v \cos \beta, \quad (2.5)$$

which we diagonalise in the usual way with the help of unitary matrices $S_{L,R}^{u,d}$,

$$u'_{L,R} = S_{L,R}^u u_{L,R}, \quad d'_{L,R} = S_{L,R}^d d_{L,R}, \quad (2.6)$$

$$S_L^{d\dagger} M^d S_R^d = \hat{M}^d = \begin{pmatrix} m_d & 0 & 0 \\ 0 & m_s & 0 \\ 0 & 0 & m_b \end{pmatrix}, \quad S_L^{u\dagger} M^u S_R^u = \hat{M}^u = \begin{pmatrix} m_u & 0 & 0 \\ 0 & m_c & 0 \\ 0 & 0 & m_t \end{pmatrix}, \quad (2.7)$$

with the unprimed fields corresponding to quark mass eigenstates. The gauge sector of the 2HDM is invariant under independent unitary rotations of the fields Q' , $d'_{L,R}$, and $u'_{L,R}$ in flavour space. We use eq. (2.6) and choose

$$Q' \equiv S_L^d Q \quad (2.8)$$

and find L_Y in the so-called *down basis*:

$$L_Y \equiv -\bar{Q} [Y^d H_d + \epsilon^d H_u] d_R - \bar{Q} [Y^u \epsilon H_u^* + \epsilon^u \epsilon H_d^*] u_R + h.c. \quad (2.9)$$

with the appropriately transformed Yukawa matrices

$$Y^{u,d} = S_L^{d\dagger} \bar{Y}^{u,d} S_R^{u,d}, \quad \epsilon^{u,d} = S_L^{d\dagger} \bar{\epsilon}^{u,d} S_R^{u,d} \quad (2.10)$$

and the CKM matrix

$$V = S_L^{u\dagger} S_L^d. \quad (2.11)$$

The Yukawa Lagrangian L_Y in eq. (2.9) is manifestly SU(2) invariant, with the SU(2) doublet

$$Q = S_L^{d\dagger} Q' = \begin{pmatrix} V^\dagger u_L \\ d_L \end{pmatrix}.$$

Eq. (2.9) is our starting point; the Yukawa matrices are related to the diagonal mass matrices as

$$\frac{\hat{M}_d}{v} = Y^d \cos \beta + \epsilon^d \sin \beta, \quad \frac{\hat{M}_u}{v} = V (Y^u \sin \beta + \epsilon^u \cos \beta). \quad (2.12)$$

Non-vanishing off-diagonal entries of $Y^{d,u}$, $\epsilon^{d,u}$ give rise to FCNC couplings of the neutral components of the Higgs doublets.

In a general 2HDM the quantity $\tan \beta$ has no physical meaning: one can arbitrarily rotate (H_u, H_d) in eq. (2.1) leading to a Lagrangian of the same form (yet with different Yukawa matrices) and the rotation angle will add to β . The situation is different in variants of the 2HDM in which H^u and H^d are distinguished by quantum numbers which forbid such rotations of (H_u, H_d) . Prominent examples are the 2HDM of type I and II, in which two out of the four Yukawa matrices in eqs. (2.1) and (2.9) are absent. The type-I model corresponds to $\epsilon^d = Y^u = 0$. The type-II model is instead found for $\epsilon^d = \epsilon^u = 0$.

The doublets $\phi_{\text{SM}}, \phi_{\text{new}}$ of the *Higgs basis* [22–24] are defined by a rotation of the two doublets H_u and H_d by the angle β such that ϕ_{new} has no vev:

$$\begin{pmatrix} \phi_{\text{new}} \\ \phi_{\text{SM}} \end{pmatrix} = \begin{pmatrix} \cos \beta & -\sin \beta \\ \sin \beta & \cos \beta \end{pmatrix} \begin{pmatrix} H_u \\ H_d \end{pmatrix} \quad (2.13)$$

One has

$$\phi_{\text{SM}} = \begin{pmatrix} G^+ \\ v + \frac{\phi^0 + iG^0}{\sqrt{2}} \end{pmatrix}, \quad \phi_{\text{new}} = \begin{pmatrix} H^+ \\ \frac{\phi^{0'} + iA^0}{\sqrt{2}} \end{pmatrix}. \quad (2.14)$$

Next we use eq. (2.13) to express L_Y in terms of ϕ_{SM} and ϕ_{new} :

$$\begin{aligned} L_Y = & \bar{Q} \left[-Y^d \cos \beta - \epsilon^d \sin \beta \right] \phi_{\text{SM}} d_R + \bar{Q} \left[Y^d \sin \beta - \epsilon^d \cos \beta \right] \phi_{\text{new}} d_R \\ & + \bar{Q} V^\dagger \left[-Y^u \sin \beta - \epsilon^u \cos \beta \right] \epsilon \phi_{\text{SM}}^* u_R \\ & + \bar{Q} V^\dagger \left[-Y^u \cos \beta + \epsilon^u \sin \beta \right] \epsilon \phi_{\text{new}}^* u_R + h.c. \end{aligned} \quad (2.15)$$

By using eq. (2.12) to eliminate Y^u and Y^d one can write the couplings to the physical charged and neutral Higgs bosons in eq. (2.15) as

$$\begin{aligned} \mathcal{L}_Y^{\text{phys}} = & -\bar{u}_L \left[\frac{\hat{M}^u}{v} \cot \beta + g^u \right] u_R \frac{\phi^{0'} - iA^0}{\sqrt{2}} + \bar{d}_L \left[\frac{\hat{M}^d}{v} \tan \beta + g^d \right] d_R \frac{\phi^{0'} + iA^0}{\sqrt{2}} \\ & + \bar{u}_L V \left[\frac{\hat{M}^d}{v} \tan \beta + g^d \right] d_R H^+ + \bar{d}_L V^\dagger \left[\frac{\hat{M}^u}{v} \cot \beta + g^u \right] u_R H^- \\ & - \bar{d}_L \frac{\hat{M}^d}{v} d_R \left(v + \frac{\phi^0}{\sqrt{2}} \right) - \bar{u}_L \frac{\hat{M}^u}{v} u_R \left(v + \frac{\phi^0}{\sqrt{2}} \right) + h.c. \end{aligned} \quad (2.16)$$

with the matrices [8]

$$g^d = -\epsilon^d \sin \beta (\tan \beta + \cot \beta), \quad g^u = -\epsilon^u \cos \beta (\tan \beta + \cot \beta). \quad (2.17)$$

The non-diagonal matrices g^d and g^u characterise the deviations from the popular type-II 2HDM (for which $g^d = g^u = 0$) and can induce flavour-changing couplings of neutral Higgs bosons. Note that the type-I model is also included in the formalism and recovered by using eq. (2.12) with $Y^u = 0$ in the expression for g^d . For our loop calculation and the phenomenological analysis it is advantageous to work with $g^{d,u}$ rather than $\epsilon^{d,u}$, especially for the definition of the renormalisation prescriptions. We write $g_{d_i d_j} \equiv g_{ij}^d$, where d_i is the i -th down-type quark flavor, $i = 1, 2, 3$, and similarly for g^u .

We restrict ourselves to the CP-conserving Higgs potential, such that A^0 is a pseudoscalar boson, while ϕ^0 and $\phi^{0'}$ are scalar particles. The two Higgs bosons ϕ^0 and $\phi^{0'}$ are in general not mass eigenstates. The latter are given by h^0 and H^0 , with

$$\begin{pmatrix} h^0 \\ H^0 \\ A^0 \end{pmatrix} = \begin{pmatrix} \sin(\beta - \alpha) & \cos(\beta - \alpha) & 0 \\ \cos(\beta - \alpha) & -\sin(\beta - \alpha) & 0 \\ 0 & 0 & 1 \end{pmatrix} \begin{pmatrix} \phi^0 \\ \phi^{0'} \\ A^0 \end{pmatrix}. \quad (2.18)$$

The angle α is a priori arbitrary, but data on decays of the 125 GeV Higgs boson constrain $\cos(\beta - \alpha)$ to be close to zero.

2.2 Spurion expansion

The 2HDM of type I and II (and their variants with modified lepton couplings) invoke (softly broken) \mathbb{Z}_2 symmetries to forbid FCNC couplings of the neutral Higgs bosons. This was motivated by the wish to find non-standard Higgs bosons at modern colliders, because for generic values of the Yukawa matrices in eq. (2.9) constraints from FCNC processes like meson-antimeson mixing push these masses to values outside the reach of LEP, Tevatron, and LHC. With the absence of discoveries of non-standard Higgs bosons this line of arguments loses its appeal and the consideration of more general Yukawa sectors is in order.

The type-II model is the most studied variant of the 2HDM for two reasons: firstly, it constitutes the tree-level Higgs sector of the Minimal Supersymmetric Standard Model (MSSM), in which the holomorphy of the superpotential enforces $\epsilon^{u,d} = 0$. Secondly, the type-II model is phenomenologically especially interesting, because in this model FCNC processes are sensitive to loop effects of the charged Higgs boson. A prominent example of the latter feature is the branching ratio $\mathcal{B}(B \rightarrow s\gamma)$, which sets a stringent bound on the charged-Higgs mass [25]. The type-II 2HDM further permits the possibility of large down-type Yukawa couplings, a scenario motivated by the possibility of bottom-top Yukawa unification. Such large- $\tan\beta$ scenarios are efficiently constrained by $\mathcal{B}(B_s \rightarrow \mu^+\mu^-)$ [26–28] and we will come back to this topic in section 5. Concerning the first above-mentioned motivation, the Higgs sector of the MSSM is really richer than that of the type-II 2HDM: in the limit of infinitely heavy superpartners one encounters non-decoupling loop-induced Yukawa matrices $\epsilon^{u,d}$, an effect caused by the supersymmetry-breaking terms [29–31]. Despite the loop suppression large effects are possible in FCNC processes with down-type quarks which involve the product $\epsilon^d \tan\beta$ [32–37] with huge impact on $\mathcal{B}(B_s \rightarrow \mu^+\mu^-)$ [32–35, 38].

The phenomenological constraints from meson-antimeson mixing and rare (semi-)leptonic decays place severe bounds on the off-diagonal elements of ϵ^d , while those of ϵ^u are essentially unconstrained except for ϵ_{12}^u and ϵ_{21}^u . This situation calls for a variant of the general 2HDM in which $Y^{u,d}$ and ϵ^u are arbitrary, while ϵ^d is suppressed. A strong motivation for such a model is the possibility of spontaneous CP violation, implemented through a Higgs potential developing complex vevs and real Yukawa matrices. Spontaneous CP violation is not possible with a 2HDM of type I or II, but requires at least three out of the four matrices in eq. (2.9) to be non-zero. Avoiding fine-tuning implies that the dominant piece of the needed effect stems from ϵ^u , while ϵ^d can be neglected [39]. However, in such a model, the mixing of the neutral Higgs fields is different from eq. (2.18) and instead involves all three fields. Yet for the CP-conserving observables considered in this paper this feature is of minor relevance. The 2HDM scenario with sizable $Y^{u,d}$ and ϵ^u has the appealing feature that it simultaneously permits both measurable effects in FCNC processes *and* sufficiently light masses of the non-standard Higgs particles enabling their discovery at the LHC.

Setting ϵ^d naively to zero leads to a non-renormalisable model, because there are UV-divergent loops involving up-type quarks with $Y^{u,d}$ and ϵ^u couplings, which require counterterms proportional to elements of ϵ^d . Whenever one seeks to constrain the elements g_{jk}^u of eq. (2.16) from FCNC transitions of down-type quarks, one must foresee such a counterterm to find a meaningful prediction. For example, $B_s \rightarrow \mu^+\mu^-$ is a $b \rightarrow s$ transition constraining g_{ct} and the corresponding loop contribution requires a counterterm for g_{sb} . The minimal

renormalisable theory is found by invoking flavour symmetries and systematically expanding in terms of the spurions breaking these symmetries [40, 41]. The 2HDM gauge sector is invariant under unitary rotations $Q \rightarrow U_Q Q$, $d_R \rightarrow U_d d_R$, $u_R \rightarrow U_u u_R$ in quark flavour space with $(U_Q, U_d, U_u) \in \text{SU}(3)^3$ and the Yukawa sector is formally invariant under this flavour symmetry if one transforms the matrices in eq. (2.9) as

$$Y^{u,d} \rightarrow U_Q Y^{u,d} U_{u,d}^\dagger, \quad \epsilon^{u,d} \rightarrow U_Q \epsilon^{u,d} U_{u,d}^\dagger. \quad (2.19)$$

We propose to categorise the classes of renormalisable 2HDM in terms of the spurions breaking the $\text{SU}(3)^3$ flavour symmetry of the quark sector.¹ The minimal choice are two spurions, with just two physically distinct possibilities. Both comply with the definition of minimal flavour violation (MFV) as defined in ref. [41]. The first possibility is to take $Y^{u,d}$ as spurions and express the other two Yukawa matrices as $\epsilon^{u,d} = P_{u,d}(Y^u Y^{u\dagger}, Y^d Y^{d\dagger}) Y^{u,d}$, where P_u and P_d are polynomials. This variant is discussed in ref. [41] and amounts to a generalisation of the 2HDM of type II. It also constitutes a renormalisable extension of the aligned 2HDM of refs. [42–44], in which $P_{u,d}$ are constants. If the 2HDM is the low-energy limit of a more fundamental theory obeying the considered two-spurion symmetry-breaking pattern, the latter will naturally induce $\epsilon^{u,d}$ in the described way as well. An example for such a UV theory is the MSSM with a flavour-blind supersymmetry breaking mechanism (such as gauge mediation). The second possibility is to choose Y^d , ϵ^u as spurions, leading to a generalisation of the type-I 2HDM.

There are two possibilities for a 2HDM with three spurions, which can be taken as $Y^{u,d}$ plus either ϵ^u or ϵ^d . The first possibility is the phenomenologically interesting one and studied in this paper. The expansion up to third order reads

$$\begin{aligned} \epsilon^d = & cY^d + c_{11}Y^d Y^{d\dagger} Y^d \\ & + b_{11}\epsilon^u \epsilon^{u\dagger} Y^d + b_{12}\epsilon^u Y^{u\dagger} Y^d + b_{21}Y^u \epsilon^{u\dagger} Y^d + b_{22}Y^u Y^{u\dagger} Y^d \end{aligned} \quad (2.20)$$

with complex coefficients c, \dots, b_{22} .

Concerning eq. (2.20) several comments are in order:

- The spurion expansion is only meaningful, if the contributions to the off-diagonal elements of ϵ^d from higher electroweak orders (with five or more Yukawa matrices) are small, so that they can be neglected. A sufficient condition for this is realised in scenarios in which c_{11}, \dots, b_{22} are induced by one-loop contributions in either the UV completion or the 2HDM, while terms with $(2n + 1)$ spurions are only generated at n -loop order and beyond. We consider this scenario throughout this paper.² Additional QCD corrections (e.g. an extra loop with a gluon) comply with the pattern in eq. (2.20), i.e. QCD renormalises the coefficients, but does not induce new ones.

¹The generalisation to the lepton sector is straightforward, but not relevant for the calculations in this paper.

²A different application of eq. (2.20), in which $c_{11}, \dots, b_{22} = \mathcal{O}(1)$ is allowed, is the case that Y^u and ϵ^u are almost aligned, so that eq. (2.12) means small off-diagonal matrix elements of these matrices in the chosen basis. Since $Y_{33}^u, \epsilon_{33}^u = \mathcal{O}(1)$ and further $Y_{33}^d = \mathcal{O}(1)$ is possible, some terms with five spurions must be added to eq. (2.20), just as in the MFV case of ref. [41].

- By rotating (H_u, H_d) in eq. (2.9) one can eliminate c in eq. (2.20). But in general radiative corrections bring this term back and a counterterm to c is needed, unless one corrects the rotation in each order of perturbation theory. It is therefore advisable to keep c in eq. (2.20); we treat it as a perturbative quantity with $c = 0$ at tree level.
- The decay $B_s \rightarrow \mu^+ \mu^-$, which is the focus of the phenomenological analysis in this paper, involves the FCNC vertex $\bar{Q}_j - d_{Rk} - H_d$ with $(j, k) = (2, 3)$. The dominant one-loop vertex diagram involves an internal H_d line and the product $Y^d Y^{d\dagger} Y^d$ or $\epsilon^u \epsilon^{u\dagger} Y^d$ stemming from the three H_d Yukawa couplings. The UV divergences can be cancelled by counterterms to c_{11} and b_{11} .
- With eq. (2.12) we can trade $Y^{u,d}$ in eq. (2.20) for the quark masses and CKM elements. Compared to the SM we find 14 additional complex parameters, the 9 entries of ϵ^u and c_{11}, \dots, b_{22} . Yet it is much more convenient to express observables in terms of g_{jk}^u of eq. (2.16) instead of ϵ_{jk}^u and then use eqs. (2.17) and (2.20) (with eq. (2.12)) to calculate the g_{jk}^d in terms of the coefficients of the spurion expansion. While this procedure is needed in a global analysis of all available data —which is beyond the scope of this paper—, the study of $b \rightarrow s$ transitions alone will simply involve g_{ct} and, with CKM suppression, g_{ut} and g_{tt} .

In a practical calculation it is cumbersome to implement the renormalisation procedure in the described way, by providing counterterms to ϵ_{jk}^u and c, \dots, b_{22} . Instead, it is much easier to renormalise the $g_{jk}^{u,d}$. If one renormalises all $g_{jk}^{u,d}$ in the $\overline{\text{MS}}$ scheme, one automatically complies with $\text{SU}(2) \times \text{U}(1)$ gauge symmetry. Therefore it is sufficient to choose the g_{jk}^d in such a way that eq. (2.20) is obeyed at tree level. In our calculation we will only need a counterterm to g_{sb} (in addition to the usual QCD counterterms for the SM parameters), if m_s is set to zero. If m_s is kept non-zero, an additional counterterm to g_{bs} is required.

In the three-spurion 2HDM the parameter $\tan \beta$ is well-defined, because unitary rotations of (H_u, H_d) would lead to $\epsilon^d \neq 0$ at tree level and spoil the spurion expansion. We are interested in phenomenologically interesting scenarios, in which the rare decays $B(B_s \rightarrow \mu^+ \mu^-)$ or $b \rightarrow s\gamma$ deviate from the SM predictions at a level probed in current and forthcoming measurements. The corresponding decay amplitudes involve a helicity flip and come with the Yukawa matrix Y^d , which grows with $\tan \beta$, so that we will consider the case that $\tan \beta$ is large. An interesting feature of the three-spurion 2HDM is that the above-mentioned amplitudes scale differently with $\tan \beta$ than in the type-II model, due to new loop contributions with g_{ct} .

Next we briefly discuss the leptonic Yukawa Lagrangian. The extremely stringent experimental bounds on FCNC transitions like $\ell_j \rightarrow \ell_k \gamma$ suggest that only one spurion is present in the lepton sector, meaning that the lepton Yukawa couplings of the two Higgs doublets are automatically diagonal in the mass eigenstate basis.³ For simplicity, we choose the leptonic Lagrangian of type-II form (i.e. we set $g^l = 0$), with the familiar $\tan \beta$ -enhanced non-standard-Higgs couplings to charged leptons:

$$\mathcal{L}_Y^l = \bar{l}_L \left[\frac{\hat{M}^l}{v} \tan \beta \right] l_R \frac{\phi^{0r} + iA^0}{\sqrt{2}} + \bar{\nu}_L \left[\frac{\hat{M}^l}{v} \tan \beta \right] l_R H^+ + h.c. \quad (2.21)$$

³We set neutrino Yukawa couplings to zero.

The diagonal mass matrix of the charged leptons is denoted by \hat{M}^l and the couplings of ϕ_{SM} are omitted in eq. (2.21).

3 The decay $B_s \rightarrow \mu^+ \mu^-$

The typical momentum scale for B_s decays is of order M_{B_s} or smaller, so that weak B_s decays can be described by an effective theory in which the heavy W, Z bosons, the top quark, and the Higgs bosons of the 2HDM are integrated out. The resulting $|\Delta B| = 1$ Hamiltonian H_{eff} describes the interactions mediated by these heavy particles in terms of dimension-6 operators changing the beauty quantum number B by one unit. The piece of H_{eff} relevant for $B_s \rightarrow \mu^+ \mu^-$ reads

$$H_{\text{eff}} = N \sum_{i=A,S,P} (C_i \bar{Q}_i + C'_i Q'_i) . \quad (3.1)$$

The operators in eq. (3.1) are

$$\begin{aligned} Q_A &= (\bar{b} \gamma_\mu P_L s) (\bar{\mu} \gamma^\mu \gamma_5 \mu) , & Q'_A &= (\bar{b} \gamma_\mu P_R s) (\bar{\mu} \gamma^\mu \gamma_5 \mu) , \\ Q_S &= (\bar{b} P_L s) (\bar{\mu} \mu) , & Q'_S &= (\bar{b} P_R s) (\bar{\mu} \mu) , \\ Q_P &= (\bar{b} P_L s) (\bar{\mu} \gamma_5 \mu) , & Q'_P &= (\bar{b} P_R s) (\bar{\mu} \gamma_5 \mu) , \end{aligned} \quad (3.2)$$

and are multiplied with their respective *Wilson coefficients* C_A, \dots, C'_P which contain the dependence on the large masses. The normalisation factor in eq. (3.1) is

$$N = \frac{G_F^2 M_W^2}{\pi^2} V_{ts} V_{tb}^* = \frac{G_F \alpha_{\text{em}}(\mu)}{\sqrt{2} \pi \sin^2 \theta_w} V_{ts} V_{tb}^* , \quad (3.3)$$

which complies with the conventions of ref. [28]. The second “=” sign only holds to lowest order in the electroweak interaction, while in higher orders the relation between the Fermi constant G_F and the electromagnetic coupling $\alpha_{\text{em}} = e^2/(4\pi)$, the weak mixing angle θ_w and the W mass M_W is modified. Electroweak corrections have been calculated in ref. [45] and e.g. remove the ambiguities related to the choice of the renormalisation scheme for these parameters; in the second version for N in eq. (3.3) this issue also includes the choice of the scale in the running α_{em} . In the following, we choose the first definition $N \propto G_F^2$ in this paper, for which the electroweak corrections to the SM contribution to C_A are as small as -2.4% [45].

We introduce the perturbative expansion of the C_i as

$$C_i = C_i^{(0)} + \left(\frac{\alpha_s}{4\pi} \right) C_i^{(1)} + \dots , \quad (3.4)$$

where $C_i^{(0)}$ denotes the leading order (LO), arising in the SM from one-loop electroweak diagrams. $C_i^{(1)}$ comprises the next-to-leading order (NLO) QCD corrections. In the SM only C_A is relevant, C'_A is suppressed w.r.t. C_A by the ratio $m_b m_s / M_W^2$ involving the strange and bottom quark masses $m_{s,b}$ and $C_{S,P}^{(l)}$ receive additional suppression factors of $M_{B_s}^2 / M_W^2$. The leading contributions $C_i^{(0)}$ arise from one-loop electroweak diagrams at order G_F^2 in the SM, hence the branching ratio is rather small.

The average time-integrated branching ratio is given by [46, 47]

$$\overline{\mathcal{B}}(B_s \rightarrow \mu^+ \mu^-) = |N|^2 \frac{M_{B_s}^3 f_{B_s}^2}{32\pi\Gamma_H^s} \beta \left[|r(C_A - C'_A) - u(C_P - C'_P)|^2 F_P + |u\beta(C_S - C'_S)|^2 F_S \right], \quad (3.5)$$

with dimensionless quantities

$$r = \frac{2m_\mu}{M_{B_s}}, \quad \beta = \sqrt{1 - r^2}, \quad u = \frac{M_{B_s}}{m_b + m_s}. \quad (3.6)$$

Here, Γ_H^s (Γ_L^s) denotes the decay width of the heavier (lighter) B_s mass eigenstate, and the factors F_P and F_S account for the mixing of the $B_s - \bar{B}_s$ system, given by

$$F_P = 1 - \frac{\Gamma_L^s - \Gamma_H^s}{\Gamma_L^s} \sin^2 [\arg(r(C'_A - C_A) - u(C'_P - C_P))],$$

$$F_S = 1 - \frac{\Gamma_L^s - \Gamma_H^s}{\Gamma_L^s} \cos^2 [\arg(C'_S - C_S)] \quad (3.7)$$

in the absence of significant CP-violating New Physics contributions to the $B_s - \bar{B}_s$ mixing amplitude. In writing eq. (3.5), we have used the pseudoscalar decay constant f_{B_s} to rewrite the operator matrix elements as

$$\langle 0 | \bar{b} \gamma_\mu \gamma_5 s | B_s(p) \rangle = i p_\mu f_{B_s},$$

$$\langle 0 | \bar{b} \gamma_5 s | B_s(p) \rangle = -i f_{B_s} \frac{M_{B_s}^2}{m_b + m_s}, \quad (3.8)$$

where the second equation follows from the first one by use of the equations of motion.

The Higgs-mediated contributions in the SM can be neglected due to the tiny Yukawa couplings of external particles. However, in the 2HDM with large Yukawa couplings of Higgs bosons to right-handed down-type quarks and leptons, Feynman diagrams with Higgs bosons are known to contribute significantly to C_S and C_P , as will be discussed in the following.

4 Computational setup

In this section, we describe the chain of programs used to generate and evaluate the corresponding Feynman diagrams at leading and next-to-leading order. We use `FeynRules` with the `Universal FeynRules Output (UFO)` [48–50] to obtain Feynman rules for the model. The output is processed by `tapir` [51] into a Lagrangian file, which is used with `qgraf` [52] in order to generate all Feynman diagrams.

We compute the one-loop diagrams for general electroweak gauge parameters for the W and Z bosons and check that they drop out in the final result. This is a welcome check for the conversion from `UFO` to `qgraf` and `tapir`. If diagrams with all different quark flavours are explicitly calculated, we have at one-loop level $< \mathcal{O}(100)$ Feynman diagrams in the SM,⁴

⁴From the technical perspective, it is convenient to split the electroweak gauge bosons into two different “particles”, with different propagator denominators $(k^2 - M^2)^{-1}$ and $(k^2 - \xi M^2)^{-1}$, respectively, and treat them as different diagrams; hence the large number of diagrams in the 1-loop calculation.

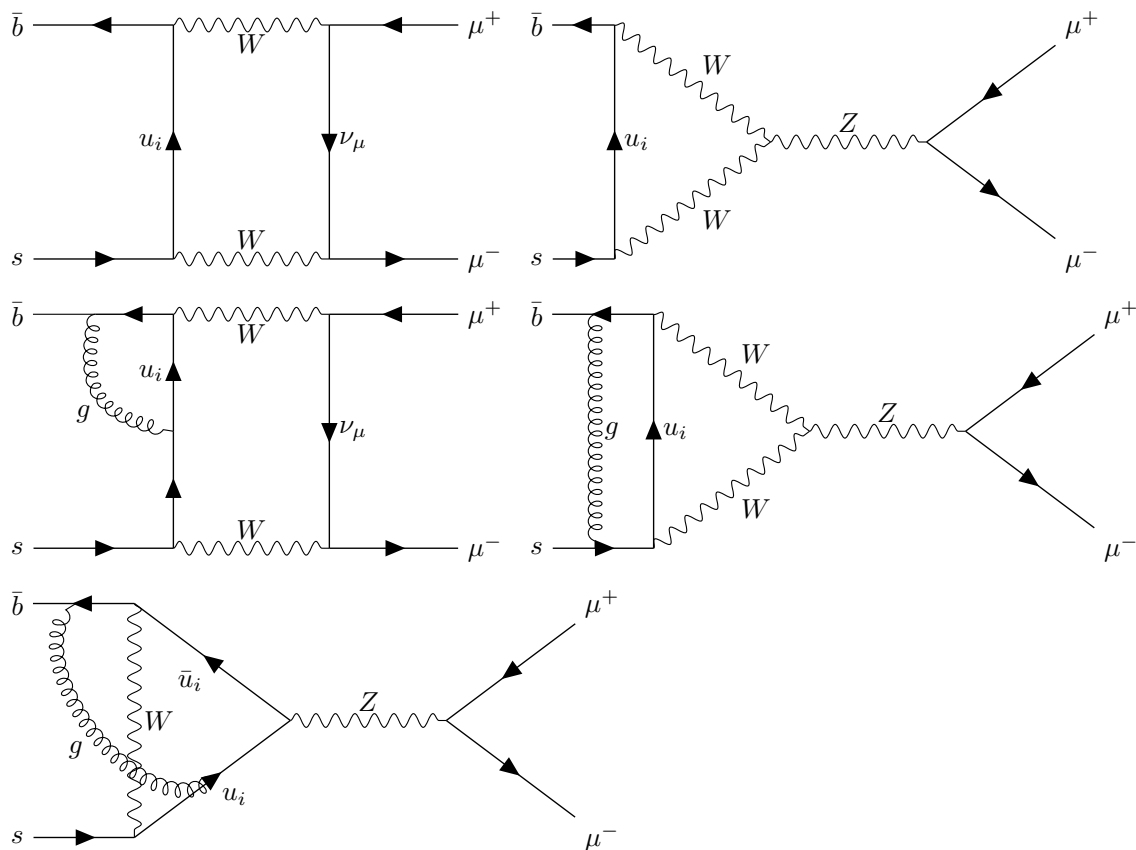


Figure 1. Sample diagrams contributing to C_A at leading and next-to-leading order in the SM.

and an additional $\mathcal{O}(300)$ diagrams from contributions with at least one non-SM Higgs boson, most of which are Higgs-penguin diagrams. At two-loop order, we perform the calculation in the Feynman gauge for the W and Z bosons, but we keep the gluon gauge parameter general and verify that it drops out of the final results.

The diagrams are then converted with the help of `tapir` into `FORM` [53] code using Feynman rule definitions that were also produced in the conversion from `UFO` to the `qgraf` Lagrangian file. The individual expressions for the diagrams are mapped onto integral families using `exp` [54, 55] and a custom `FORM` setup is used to perform the remaining computational steps. Since the Wilson coefficients are independent of the momenta of the external particles, we set the latter to zero, so that only vacuum integrals need to be computed. (An exception are diagrams with an FCNC self-energy in an external leg, which are calculated with on-shell b quark and $m_b \neq 0$ before the subsequent limit $m_b \rightarrow 0$ is taken.) We use a `FORM` implementation of the algorithm presented in ref. [56], see ref. [57].

5 The decay $B_s \rightarrow \mu^+ \mu^-$ in the two-Higgs-doublet model of type-II

In the SM the leading-order result was obtained in ref. [58] and next-to-leading order QCD corrections have been presented in refs. [59–62]. Higher-order QCD and electroweak corrections have been computed in refs. [27, 28, 45, 63, 64]. Next-to-leading corrections in the type-II

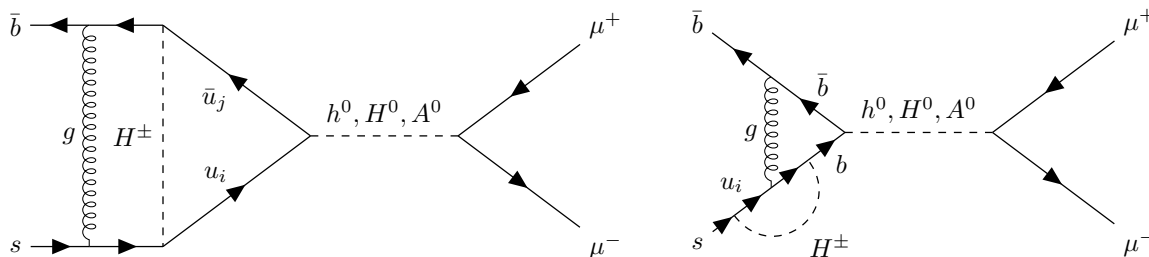


Figure 2. Sample two-loop Feynman diagrams contributing to the Wilson coefficients $C_S^{(I)}$ ($H_{1,2}$) and $C_P^{(I)}$ (A^0). In the left diagram, only flavour-diagonal transitions $i = j$ are possible in the type-II 2HDM, while the more general 2HDM allows also for transitions with $i \neq j$, e.g. transitions from a charm quark into a top quark.

2HDM have been calculated in refs. [26, 65–67]. We have reproduced these results for the present paper, also as a check of the automated setup. The result can be expressed in terms of dimensionless mass ratios of the top quark, W boson and charged Higgs boson masses,

$$x_t = \frac{m_t^2}{M_W^2}, \quad r_H = \frac{m_t^2}{M_{H^\pm}^2}. \quad (5.1)$$

In the SM, only the Wilson coefficient C_A receives significant contributions from diagrams such as the ones depicted in figure 1. The Wilson coefficients C'_A, C_S, \dots, C'_P are suppressed by powers of ratios of light (external) masses and M_W . The leading SM contribution is, moreover, independent of the Yukawa couplings of all external particles, that is we can set $m_b = m_s = m_\mu = 0$ for the contributions from W -box and Z -penguin diagrams. At leading and next-to-leading order they are given by

$$C_A^{W+Z,(0)} = \frac{x_t(x_t - 4)}{8(x_t - 1)} + \frac{3x_t^2 \log x_t}{8(x_t - 1)^2}, \quad (5.2)$$

$$C_A^{W+Z,(1)} = \frac{2x_t(2x_t^2 + 5x_t + 5)}{3(x_t - 1)^2} - \frac{x_t(x_t^2 + 5x_t + 2) \log x_t}{(x_t - 1)^3} - \frac{x_t(x_t^2 + 2) \text{Li}_2\left(1 - \frac{1}{x_t}\right)}{(x_t - 1)^2} + \left(\frac{x_t(x_t^2 + x_t + 4)}{(x_t - 1)^2} - \frac{6x_t^2 \log x_t}{(x_t - 1)^3} \right) \log \frac{\mu^2}{m_t^2}, \quad (5.3)$$

where the Z -penguin contributions include the flavour-changing quark self-energy diagrams required to make the penguin diagrams finite. Moreover, since charm and up quark masses can be neglected compared to M_W and m_t , after summation over internal up-type quarks all contributions are proportional to the CKM factor $V_{ts}V_{tb}^*$ (contained in the normalisation factor N defined in eq. (3.3)) due to the unitarity of the CKM matrix.

In the 2HDM of type-II the leading new effects stem from $\mathcal{O}(\tan^2 \beta)$ contributions to $C_S^{(I)}$ and $C_P^{(I)}$, arising from penguin diagrams with a neutral Higgs boson, see e.g. figure 2, and the W^+-H^\pm box diagram [26]. The Higgs-penguin contributions to C_S are given in Feynman gauge for the W -boson by

$$C_S^{h,(0)} = -r_b \left[\frac{r_H x_t \log r_H}{4(r_H - 1)(r_H - x_t)} - \frac{r_H x_t \log x_t}{4(x_t - 1)(r_H - x_t)} \right], \quad (5.4)$$

$$\begin{aligned}
 C_S^{h,(1)} = & -r_b \left[-\frac{8r_H x_t}{3(r_H-1)(x_t-1)} + \frac{2r_H x_t(3r_H-7)\log r_H}{3(r_H-1)^2(r_H-x_t)} - \frac{2r_H x_t(3x_t-7)\log x_t}{3(x_t-1)^2(r_H-x_t)} \right. \\
 & - 2 \log\left(\frac{\mu^2}{m_t^2}\right) \left(\frac{r_H x_t}{(r_H-1)(x_t-1)} + \frac{r_H x_t \log r_H}{(r_H-1)^2(r_H-x_t)} - \frac{r_H x_t \log x_t}{(x_t-1)^2(r_H-x_t)} \right) \\
 & \left. + \frac{2r_H x_t \text{Li}_2\left(1 - \frac{1}{r_H}\right)}{r_H - x_t} - \frac{2r_H x_t \text{Li}_2\left(1 - \frac{1}{x_t}\right)}{r_H - x_t} \right], \tag{5.5}
 \end{aligned}$$

where

$$r_q = \frac{m_\mu m_q \tan^2 \beta}{M_W^2}. \tag{5.6}$$

The Wilson coefficients for the right-handed operators $C_S^{h,(i)}$ can be obtained by the replacement $r_b \rightarrow r_s$ in eqs. (5.4) and (5.5). Further contributions include terms of order $m_b m_s m_\mu^2 \tan^4 \beta / M_W^4$ and $m_t^2 m_\mu^2 / M_W^4$ entering the Wilson coefficients C'_A and C_A , respectively, as well as $\mathcal{O}(m_b m_s \tan^2 \beta / M_W^2)$ (in C'_A) and $\mathcal{O}(m_t^2 \cot^2 \beta / M_W^2)$ (in C_A) terms arising from Z -penguin diagrams with a charged Higgs boson. Box diagrams with a single charged Higgs boson also contribute to $C_{S,P}$ ($C'_{S,P}$), with Wilson coefficients proportional to m_b (m_s). We do not explicitly list these contributions here; they can be found in refs. [65–67]. With the exception of the doubly muon-mass suppressed H^+H^- box contributions to C_A , we include all of these additional terms in our analysis. The feature that C_S and C_P are proportional to m_b while their primed counterparts are proportional to m_s holds beyond the type-II 2HDM in our more general 2HDM with three spurions because of $\epsilon^d = P_d(\epsilon^u, Y^u, Y^d)Y^d$, entailing factors of m_{d_j} in Yukawa couplings of d_{jR} . A rather remarkable feature of the type-II 2HDM is the fact that the leading terms in $\tan \beta$ depend only on $\tan \beta$ and the charged-Higgs boson mass M_{H^\pm} , that is they are independent of the parameters of the neutral Higgs sector [26]. In the type-II 2HDM, the leading $\tan^2 \beta$ contributions to the pseudoscalar and scalar Wilson coefficients satisfy the rather simple relation

$$C_S = C_P, \quad C'_S = -C'_P. \tag{5.7}$$

In figure 3 we show the branching ratio $\mathcal{B}(B_s \rightarrow \mu^+ \mu^-)$ in the type-II 2HDM as a function of the charged Higgs boson mass. The horizontal green, grey, and violet bands correspond to the experimental measurements of LHCb [85] and CMS [70] as well as the theory prediction [27], respectively, including 2σ uncertainties for the experimental values (cf. table 1). The theory prediction of ref. [27] uses $|V_{cb}| = 0.0424 \pm 0.0009$, which is close to today's value inferred from inclusive $b \rightarrow c \ell \nu$ decays. If one uses $|V_{cb}| = 0.03936 \pm 0.00068$ from exclusive B decays [86] the central value of the theory prediction for $10^9 \mathcal{B}(B_s \rightarrow \mu^+ \mu^-)$ drops from 3.65 to 3.15.

The coloured lines are predictions from the 2HDM for different values of $\tan \beta$. It is interesting to note that for $\tan \beta \lesssim 25$ low values of M_{H^\pm} are required to reproduce the central value of the LHCb measurement. Of course, in the limit $M_{H^\pm} \rightarrow \infty$ all 2HDM curves approach the SM prediction. Note that in the type-II model there is a $\tan \beta$ -independent 95% C.L. lower bound on M_{H^\pm} in the range 570–800 GeV from $B \rightarrow X_s \gamma$ [25]. This bound can be easily weakened with our model's additional couplings discussed in the following section.

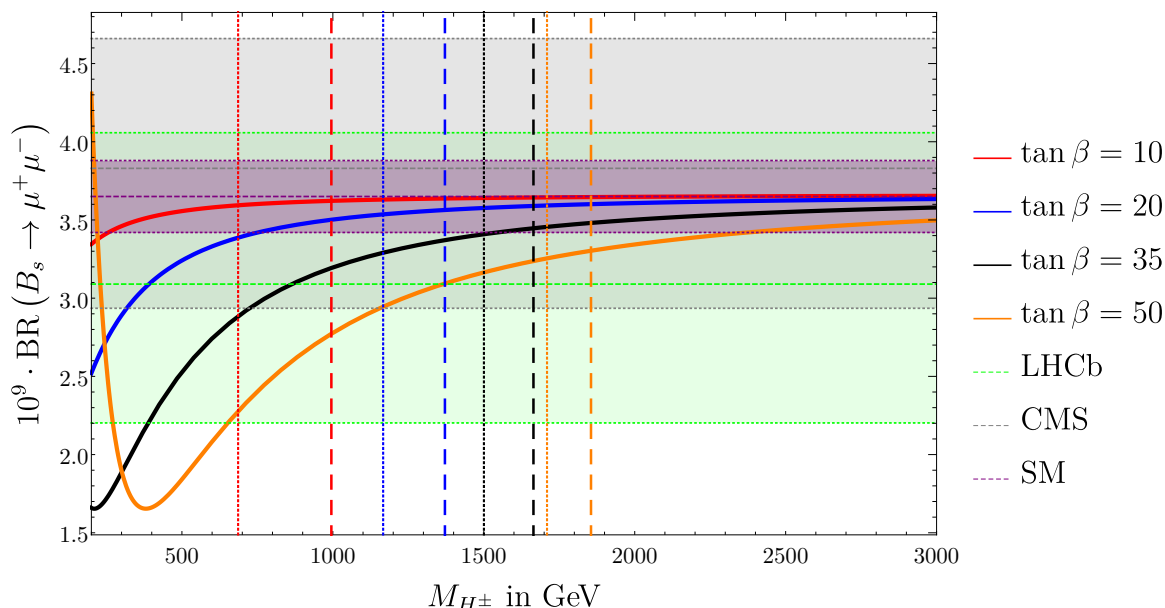


Figure 3. Branching ratio $\mathcal{B}(B_s \rightarrow \mu^+ \mu^-)$ in the type-II Two-Higgs-Doublet model at next-to-leading order in QCD, for different values of $\tan \beta$. All running parameters are evaluated at the scale $\mu = \bar{m}_t(\bar{m}_t)$. The green dashed and dotted lines denote the central value and the experimental 2σ error of the LHCb measurement [68, 69], respectively, the grey band shows the corresponding information for the CMS result [70]. The purple dashed and dotted bands indicate the SM prediction with uncertainties, presented in ref. [27]. Note that the SM prediction in the purple band was obtained including also $\mathcal{O}(\alpha_s^2)$ and $\mathcal{O}(\alpha_{\text{em}})$ contributions and corresponds to $|V_{cb}| = 0.0424 \pm 0.0009$. The perturbativity of the scalar 2HDM potential constrains $|M_{A^0}^2 - M_{H^\pm}^2| \leq |\lambda_4 - \lambda_5|v^2 \lesssim 8v^2$ [71–84], which can be converted into a lower bound on M_{H^\pm} by use of the experimentally excluded area of the $(M_{A^0}, \tan \beta)$ plane such as the ones shown in figure 9 used by us. The vertical dashed lines indicate these lower limits on M_{H^\pm} for each value of $\tan \beta$, whereas the vertical dotted lines show the same limits obtained with the less stringent constraint $|\lambda_4 - \lambda_5| \leq 8\pi$. The plot shows that $B_s \rightarrow \mu^+ \mu^-$ will only give constraints on the type-II 2HDM competitive with the Higgs searches, once the experimental precision on $\mathcal{B}(B_s \rightarrow \mu^+ \mu^-)$ substantially improves.

Recently it has been pointed out that LHC data still permit $M_{H^\pm} \leq 400$ GeV with couplings compatible with solutions of the $b \rightarrow c\tau\nu$ flavour anomalies [87, 88]. Charged-Higgs explanations of the latter have been found viable in refs. [89, 90] and are invigorated by recent LHCb data on $B \rightarrow D^{(*)}\tau\nu$ [91], see refs. [92, 93]. It should be clearly stated that this solution to the $b \rightarrow c\tau\nu$ puzzle is not realised in the type-II model, in which for instance $\mathcal{B}(b \rightarrow c\tau\nu)$ is suppressed rather than enhanced over $\mathcal{B}(b \rightarrow c\mu\nu)$ as preferred by data. Also while charged Higgs searches at the LHC are compatible with the quoted H^\pm masses [94], the lower bound on M_{H^\pm} inferred from the data on $gg/b\bar{b} \rightarrow A^0[\rightarrow \tau^+\tau^-]$ searches is larger than 1 TeV [95] in perturbed versions of the type-II 2HDM. Also in our model we cannot substantially weaken this bound; to this end one must modify the A^0 coupling to τ 's by deviating from the type-II form in eq. (2.21) and permitting the third lepton generation to couple to the other Higgs doublet.

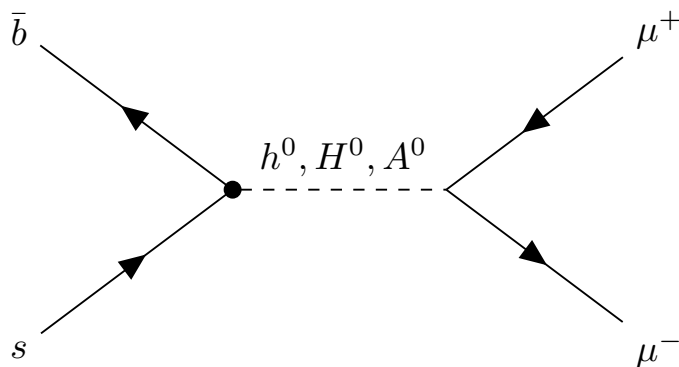


Figure 4. Tree-level diagrams with flavour-changing neutral Higgs couplings. The $b - s - H$ coupling is denoted by a dot on the vertex.

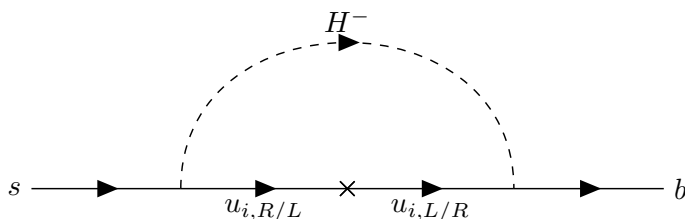


Figure 5. The loop-induced change of flavours $s \rightarrow b$ via a quark self-energy diagram. The helicity flip denoted by the cross entails a factor of $\tan \beta$ and linearity in \hat{g}^u .

6 Additional contributions in a model with flavour-changing neutral Yukawa couplings

In a model with a Yukawa Lagrangian given by eq. (2.16) there are additional tree-level contributions $\bar{b}s \rightarrow h^0(H^0, A^0) \rightarrow \mu^+\mu^-$ of order $\tan \beta$. A sample Feynman diagram is shown in figure 4. At loop-level there are $\mathcal{O}(\tan^3 \beta)$ terms due to diagrams in which the neutral Higgs boson couples to the b line. At LO these are diagrams with a FCNC self-energy and we also refer to them as self-energy diagrams at NLO, even if a gluon connects the FCNC loop with the s quark as in the diagram on the right in figure 2. These $\mathcal{O}(\tan^3 \beta)$ terms occur because a $\tan \beta$ -enhanced coupling in the self-energy diagrams is not cancelled by a factor $\cot \beta$ in the second charged-Higgs coupling, which is a distinguishing feature compared to the type-II model. If these self-energy diagrams involve a helicity flip of the internal fermion line, see figure 5, they come with a factor of $\tan \beta$ and are linear in the flavour-changing Yukawa matrix g^u , which enters the result through the charged-Higgs coupling in the fourth term of eq. (2.16). In fact, the dominant dependence on g_{ct} stems from this source and not from diagrams in which a neutral Higgs boson couples to charm and top in a vertex diagram, which have a factor of $\tan \beta$ less. Note that contributions from diagrams without helicity flip are either already included in the type-II model or quadratic in g^u (and without the factor $\tan \beta$), and we will consequently neglect the latter in what follows.

6.1 Pseudoscalar Wilson coefficient C_P

At tree level the Wilson coefficient C_P originating from the diagram in figure 4 with a virtual A^0 boson is given by

$$C_P^{(0),\text{tree}} = -\frac{\pi^2}{G_F^2 M_W^2 V_{tb}^* V_{ts}} \frac{m_\mu \tan \beta}{2v M_{A^0}^2} g_{sb}^* = -\frac{g_{sb}^*}{g_{bs}} C_P^{\prime(0)}. \quad (6.1)$$

Since there is no loop-suppression, even small values of g_{bs} and g_{sb}^* can have significant impact on the branching ratio, but the spurion expansion in eq. (2.20) naturally leads to (parametrically suppressed) small couplings. For convenience, let us define the linear combinations $g_{bs}^\pm \equiv g_{bs} \pm g_{sb}^*$.

At one-loop order only the self-energy diagrams contain an enhancement factor $\tan^3 \beta$ whereas the vertex contributions contain at most a quadratic term. The one-loop self-energy contributions to C_P and C_P' are ultra-violet divergent. The corresponding counterterm is generated from eq. (6.1) and is of the form

$$g_{bs}^{+,0} = g_{bs}^+ + \delta_{A^0,bs}^{+(0)} + \left(\frac{\alpha_s}{4\pi}\right) \delta_{A^0,bs}^{+(1)} + \dots \quad (6.2)$$

In the $\overline{\text{MS}}$ renormalisation scheme the one-loop contribution is given by

$$\delta_{A^0,bs}^{+(0)} = -\frac{1}{\epsilon} \frac{\sqrt{2} G_F m_t \tan^2 \beta}{8\pi^2} [(g_{ut}^* V_{us} + g_{ct}^* V_{cs} + g_{tt}^* V_{ts}) m_b V_{tb}^* + (g_{ut} V_{ub}^* + g_{ct} V_{cb}^* + g_{tt} V_{tb}^*) m_s V_{ts}]. \quad (6.3)$$

Defining analogously

$$g_{bs}^{-,0} = g_{bs}^- + \delta_{A^0,bs}^{-(0)} + \left(\frac{\alpha_s}{4\pi}\right) \delta_{A^0,bs}^{-(1)} + \dots, \quad (6.4)$$

the counterterms $\delta_{A^0,bs}^{-(0)}$ and $\delta_{A^0,bs}^{-(1)}$ are found from $\delta_{A^0,bs}^{+(0)}$ and $\delta_{A^0,bs}^{+(1)}$ in eqs. (6.3) and (6.8) below by the replacement $m_b \rightarrow -m_b$. Thus the terms with m_b renormalise the Wilson coefficient $C_P \propto g_{bs}^+ - g_{bs}^-$, while the ones with m_s renormalise the Wilson coefficient $C_P' \propto -(g_{bs}^+ + g_{bs}^-)$. The renormalised finite pseudoscalar Wilson coefficients read

$$\begin{aligned} C_P^{(0)} &= C_P^{(0),\text{tree}} + \tilde{N} \frac{m_b}{M_{A^0}^2} \left(g_{ut}^* \frac{V_{us}}{V_{ts}} + g_{ct}^* \frac{V_{cs}}{V_{ts}} + g_{tt}^* \right) \tilde{C}_P^{(0)}, \\ C_P^{\prime(0)} &= C_P^{\prime(0),\text{tree}} - \tilde{N} \frac{m_s}{M_{A^0}^2} \left(g_{ut} \frac{V_{ub}^*}{V_{tb}^*} + g_{ct} \frac{V_{cb}^*}{V_{tb}^*} + g_{tt} \right) \tilde{C}_P^{(0)}, \end{aligned} \quad (6.5)$$

with normalisation factor

$$\tilde{N} = \frac{m_t m_\mu \tan^3 \beta}{G_F \sqrt{2} M_W^2 v} = \frac{g m_t m_\mu \tan^3 \beta}{2 G_F M_W^3}, \quad (6.6)$$

the weak coupling constant g , and

$$\tilde{C}_P^{(0)} = -\frac{1}{8} \left[1 + \log \frac{\mu^2}{m_t^2} - \frac{\log r_H}{r_H - 1} \right]. \quad (6.7)$$

Our results in eqs. (6.1)–(6.7) confirm the result in eq. (3.16) of ref. [9]. At NLO in QCD (i.e. two-loop order), the counterterm required to obtain a finite result is given by

$$\delta_{A^0, sb}^{(1)} = -\frac{G_F m_t \tan^2 \beta}{\sqrt{2}\pi^2} \left[(g_{ut}^* V_{us} + g_{ct}^* V_{cs} + g_{tt}^* V_{ts}) m_b V_{tb}^* + (g_{ut} V_{ub}^* + g_{ct} V_{cb}^* + g_{tt} V_{tb}^*) m_s V_{ts} \right] \times \left[\frac{1}{\epsilon^2} + \frac{4}{3\epsilon} \right]. \quad (6.8)$$

Note that in addition to the top quark mass m_t also the flavour-changing Yukawa couplings are minimally renormalised. The two-loop contribution to the Wilson coefficients reads

$$\begin{aligned} C_P^{(1)} &= \tilde{N} \frac{m_b}{M_{A^0}^2} \left(g_{ut}^* \frac{V_{us}}{V_{ts}} + g_{ct}^* \frac{V_{cs}}{V_{ts}} + g_{tt}^* \right) \tilde{C}_P^{(1)}, \\ C_P^{\prime(1)} &= -\tilde{N} \frac{m_s}{M_{A^0}^2} \left(g_{ut} \frac{V_{ub}^*}{V_{tb}^*} + g_{ct} \frac{V_{cb}^*}{V_{tb}^*} + g_{tt} \right) \tilde{C}_P^{(1)}, \end{aligned} \quad (6.9)$$

with

$$\begin{aligned} \tilde{C}_P^{(1)} &= -\frac{4(r_H - 2)}{3(r_H - 1)} + \frac{(3r_H - 7) \log(r_H)}{3(r_H - 1)^2} + \left(\frac{7 - 4r_H}{3(r_H - 1)} - \frac{\log(r_H)}{(r_H - 1)^2} \right) \log \left(\frac{\mu^2}{m_t^2} \right) \\ &\quad - \frac{1}{2} \log^2 \left(\frac{\mu^2}{m_t^2} \right) + \text{Li}_2 \left(1 - \frac{1}{r_H} \right). \end{aligned} \quad (6.10)$$

Next we discuss the dependence of our result on the renormalisation scale μ at which the 2HDM result is matched to the effective $|\Delta B| = 1$ Hamiltonian and the size of higher-order corrections. In the case $m_t \sim M_{H^+}$ the choice $\mu = \mathcal{O}(m_t, M_{H^+})$ leads to the absence of large logarithms and the variation of μ between m_t and M_{H^+} does not constitute a relevant source of theoretical uncertainty. Thus we are left to the phenomenologically interesting case $M_{H^+} \gg m_t$. The $\log \mu^2$ terms in the Wilson coefficients have two different origins, divergent contributions involving Yukawa couplings or the QCD coupling, respectively. $C_P^{(0)}$ stems from a loop with Yukawa couplings and $C_P^{(0)}$ involves no large logarithm for the choice $\mu \sim M_{H^+}$. To verify this expand eq. (6.7) as

$$\tilde{C}_P^{(0)} = -\frac{1}{8} \left(1 + \log \frac{\mu^2}{M_{H^+}^2} \right) (1 + \mathcal{O}(r_H)). \quad (6.11)$$

This feature is generic for all $\log \mu^2$ terms stemming from loops with Yukawa couplings, because heavy particles like H^+ do not contribute to the renormalisation group functions (i.e. β functions and anomalous dimensions) for $\mu < M_{H^+}$ since heavy particles are integrated out at scales of the order of their masses. The same loop diagrams yielding $\tilde{C}_P^{(0)}$ also determine the piece of the β functions of g_{sb} proportional to the Yukawa couplings of top and bottom quarks. The running of $g_{sb}(\mu)$ from this source is compensated by the explicit logarithm in eq. (6.11) and the remaining Yukawa- μ dependence is a tiny two-loop effect.

The situation is different with the μ dependence stemming from gluon loops and related to the familiar QCD running of couplings and quark masses. The QCD running of g_{sb} is trivial, since the combination $g_{sb}(\mu)/m_b(\mu)$, which enters $C_P \cdot \langle Q_P \rangle$, is independent of μ (see eq. (3.8)). To study the μ dependence of our two-loop result $C_P^{(1)}$, we keep the $\log \mu^2$ term

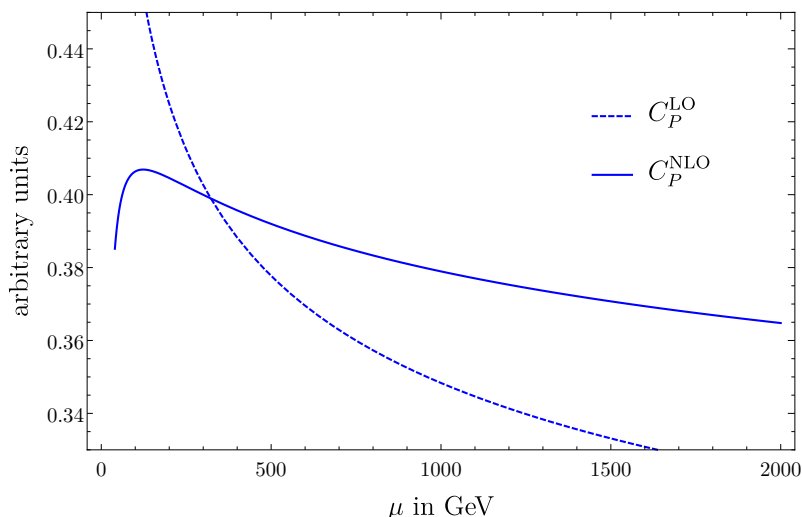


Figure 6. QCD scale dependence of the Wilson coefficient C_P at leading and next-to-leading order in α_s . In this plot we have used $M_{H^+} = 1.5$ TeV and $g_{ct}(\bar{m}_t) = 1$ and have further set $V_{ts}/V_{cs} \rightarrow 0$. All μ -independent prefactors have been fixed. $C_P(\mu)$ depends logarithmically on the masses m_t and M_{H^+} , so that every choice of μ in the interval $[m_t, M_{H^+}]$ seems justified. The plot shows, however, that choosing $\mu \sim M_{H^+}$ in $C_P^{(0)}(\mu)$ would badly underestimate the NLO result, while $\mu \sim m_t$ would sizably overestimate it. $C_P^{(0)}(m_t)$ exceeds $C_P^{(0)}(M_{H^+})$ by 24%, while the corresponding value for $C_P^{(1)}(\mu)$ is 9%.

stemming from the Yukawa interaction (i.e. the analogue of the logarithm in eq. (6.11)) fixed and vary μ otherwise. $C_P^{(0)}$ depends on μ implicitly through the μ -dependence of m_t and g_{it} and this dependence should be compensated by the explicit $\log \mu^2$ terms in $C_P^{(1)}$, reducing the μ -dependence to the three-loop (one-loop Yukawa correction and NNLO QCD) level.⁵ In figure 6 we illustrate the QCD scale dependence of the $\mathcal{O}(\alpha_s^0)$ and $\mathcal{O}(\alpha_s)$ Wilson coefficient C_P for a particular choice of M_{H^+} and $g_{ct} \equiv g_{ct}(\bar{m}_t)$. All parameters that are not running in QCD have been fixed in this figure and we have neglected the contributions from g_{ut} and g_{tt} , which have the same running as g_{ct} , such that the only running parameters are in $m_t g_{ct}^* \tilde{C}_P^{(0,1)}$. The figure shows a significant improvement of the QCD scale dependence with the inclusion of next-to-leading order QCD corrections. The LO result does not permit a reliable prediction of C_P , while C_P^{NLO} merely changes by $\pm 5\%$ around its central value when μ is varied between m_t and M_{H^+} .

From figure 6 it is clear that our calculated QCD corrections are needed for a reliable prediction. Next we discuss uncalculated higher-order corrections involving Yukawa couplings, obtained by dressing the LO diagrams with an additional Higgs boson. The large $\mathcal{O}(1)$ couplings are the coupling of the SM-like Higgs boson h^0 to the top quark and the A^0, H^0 couplings to the bottom quark.⁶ The former contributions are already present in the SM, contained in the electroweak corrections of ref. [45]. Since they are very small in the SM, they

⁵The scale dependence of the light quark mass $m_b(\mu)$ in C_P is a relic of our choice of definition of the effective operators, and will be cancelled by the corresponding running of the hadronic matrix element, see eq. (3.8). Thus, we do not consider the running of m_b in the following.

⁶While a priori the couplings of ϕ_{new} to up-type quarks could be $\geq \mathcal{O}(1)$, we will see in section 7 that in the phenomenologically interesting parameter region they are smaller.

will constitute an even smaller correction to the extra diagrams of the 2HDM. The dominant contribution from an extra loop with A^0 or H^0 is expected from diagrams in which both ends of the additional Higgs line are connected to a b line. Contrary to the QCD case, all A^0 , H^0 diagrams involve momenta which are far off-shell, because M_{A^0, H^0} is much larger than m_b . Thus the additional loop will give a correction in the few-% region to the leading 2HDM term, which is numerically constrained to the range between SM prediction and experimental value and thereby constitute a small correction to a small LO 2HDM term.

6.2 Scalar Wilson coefficient C_S

The scalar Wilson coefficients receives contributions from both neutral CP-even Higgs mass eigenstates h^0 and H^0 . At tree level, the diagrams with h^0 and H^0 give rise to the Wilson coefficients

$$C_S^{(0), \text{tree}} = -\frac{\pi^2}{G_F^2 M_W^2 V_{tb}^* V_{ts}} \frac{m_\mu \tan \beta}{2v} R_M g_{sb}^* = \frac{g_{sb}^*}{g_{bs}} C_S^{\prime(0)}, \quad (6.12)$$

where

$$R_M = \frac{M_{h^0}^2 \sin^2(\beta - \alpha) + M_{H^0}^2 \cos^2(\beta - \alpha)}{M_{h^0}^2 M_{H^0}^2} \quad (6.13)$$

contains the dependence on the neutral Higgs-boson masses. The counterterms required to cure the divergences at one and two loops can be obtained from eqs. (6.3) and (6.8) analogously, i.e. the combination $g_{bs}^+ - g_{bs}^-$ renormalises C_S , while the combination $g_{bs}^+ + g_{bs}^-$ renormalises C_S' . The renormalised Wilson coefficients C_S and C_S' are related to the pseudoscalar ones by

$$C_S^{(i)} = R_M M_{A^0}^2 C_P^{(i)}, \quad C_S^{\prime(i)} = -R_M M_{A^0}^2 C_P^{\prime(i)}. \quad (6.14)$$

Note that there are no QCD corrections to $C_{S,P}^{(i), \text{tree}}$ since they cancel in the matching calculation.

7 Phenomenology

In this section we discuss the possible size of $\mathcal{B}(B_s \rightarrow \mu^+ \mu^-)$ in our 2HDM under the constraint that other $b \rightarrow s$ processes comply with the data. We include the tree-level contributions from diagrams with flavour-changing down-type couplings (cf. figure 4), as well as the SM results and the leading quadratic $\tan \beta$ contributions in the type-II 2HDM to which the additional diagrams of order $\tan^3 \beta$ discussed in the previous section add as corrections.

In a generic 2HDM the tree-level couplings g_{bs}^\pm will drastically increase the branching ratio for $B_s \rightarrow \mu^+ \mu^-$ due to the missing loop suppression. In our model the spurion expansion suppresses g_{bs}^\pm in a controlled way, but still permits large enough contributions to get phenomenologically interesting effects in $B_s \rightarrow \mu^+ \mu^-$: even rather small up-type couplings g_{ct} significantly modify the Wilson coefficients $C_P^{(l)}$ and $C_S^{(l)}$, as they feature a CKM factor V_{cs} instead of V_{ts} . In the following, we will restrict ourselves to the experimentally favoured scenario [96, 97] of aligned Higgs doublets, in which $\sin(\beta - \alpha) \approx 1$. For the numerical analysis, we will set $\sin(\beta - \alpha) = 1$, and therefore have $R_M = M_{H^0}^{-2}$. In this case, the Higgs mass eigenstates h^0 and H^0 coincide with ϕ^0 and $-\phi^{0'}$, respectively, and only the latter possesses non-SM-like couplings to fermions. This reduces the number of relevant non-Yukawa-type parameters of the extended Higgs sector to four, namely $\tan \beta$, M_{H^+} , M_{A^0} and $M_{\phi^{0'}} \equiv M_{H^0}$.

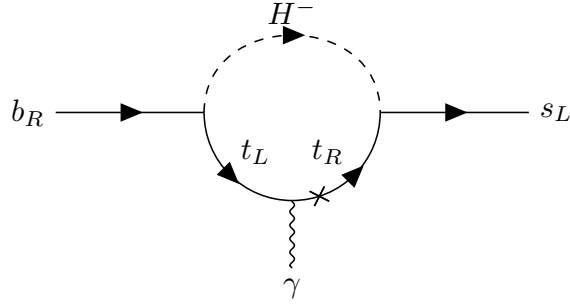


Figure 7. Sample Feynman diagram for the rare decay $b \rightarrow s\gamma$ at one loop in the 2HDM. The cross indicates a chirality flip $t_L \rightarrow t_R$.

7.1 Constraints from $b \rightarrow s\gamma$ decays

An important constraint on the magnitude of flavour-changing Yukawa couplings in the up-type quark sector arises from the inclusive rare decays $B \rightarrow X_s\gamma$. This process is mediated at the quark level by $b \rightarrow s\gamma$ through a top quark loop with a charged W boson in the Standard Model and receives additional contributions through charged-Higgs boson diagrams in the 2HDM, see figure 7. In order to eliminate the dependence on $V_{cb} \simeq -V_{ts}$, one traditionally works with the quantity

$$R_\gamma \equiv \frac{\mathcal{B}(b \rightarrow s\gamma) + \mathcal{B}(b \rightarrow d\gamma)}{\mathcal{B}(b \rightarrow c\nu)}. \quad (7.1)$$

Note that in the SM and the type-II 2HDM the branching ratio of $b \rightarrow d\gamma$ is much smaller than that of $b \rightarrow s\gamma$.

In the type-II 2HDM, the contribution of the charged Higgs diagrams to the decay rate is positive, moving the theoretical prediction for the branching ratio away from the experimental value averaged in [25] to

$$R_{\gamma,\text{exp.}} = (3.22 \pm 0.15) \cdot 10^{-3}, \quad (7.2)$$

where a lower cutoff of $E_0 \geq 1.6 \text{ GeV}$ has been put on the photon energy. The practical independence of R_γ of $\tan\beta$ in the largest part of the parameter space in the type-II 2HDM allowed for the extraction of a lower limit on the mass of the charged Higgs boson in [25], see section 5. In the general 2HDM, where, contrary to the type-II case, the factor $\tan\beta$ from the btH^- vertex is not cancelled by a factor $\cot\beta$ from the stH^- vertex, the quantity R_γ depends on $\tan\beta$.⁷ The combination of the $\bar{t}_L b_R H^+$ and $\bar{s}_L t_R H^-$ Yukawa couplings arising in the process is then given by

$$\left(\frac{m_b \tan\beta V_{tb}}{v} \right) \left(\frac{m_t V_{ts}^*}{v \tan\beta} + V_{us}^* g_{ut} + V_{cs}^* g_{ct} + V_{ts}^* g_{tt} \right) = \frac{m_b m_t V_{tb} V_{ts}^*}{v^2} (1 + g_{st}^{\text{eff}}), \quad (7.3)$$

where we have defined the short-hand notation

$$g_{st}^{\text{eff}} \equiv \frac{v \tan\beta}{m_t} \left(g_{ut} \frac{V_{us}^*}{V_{ts}^*} + g_{ct} \frac{V_{cs}^*}{V_{ts}^*} + g_{tt} \right). \quad (7.4)$$

⁷The absence of the $\cot\beta$ suppression of the stH^- vertex is also a feature of the aligned 2HDM [98–100].

Note that g_{st}^{eff} carries a factor of $\tan\beta$. The abbreviation g_{st}^{eff} denotes the size of the additional $\bar{s}_L t_R H^+$ coupling of our three-spurion 2HDM (terms involving g_{ij}^u) in units of the same coupling in the type-II 2HDM (denoted by “1” in eq. (7.3)). Thus, the limiting case of the type-II 2HDM is given by $g_{st}^{\text{eff}} = 0$, while our effective H^\pm coupling vanishes for $g_{st}^{\text{eff}} = -1$, i.e. $g_{st}^{\text{eff}} = -1$ must be chosen to recover the SM result for R_γ . We further note that g_{st}^{eff} is dominated by g_{ct} due to the large ratio $|V_{cs}/V_{ts}|$, and neglecting subleading CKM-matrix elements (amounting to set to zero g_{tt} and g_{ut} , which is instead constrained by $b \rightarrow d$ processes) allows to convert constraints on g_{st}^{eff} into bounds on g_{ct} in the following discussion.

In order to constrain our new flavour-changing couplings, we use the results from [101] and [25] with this trivial change of the $\bar{s}_L t_R H^-$ Yukawa coupling. For large enough values of M_{H^\pm} , the central value of R_γ is approximately given (at $\mu = \bar{m}_t(\bar{m}_t)$) by

$$\begin{aligned}
 R_\gamma \approx 10^{-4} \cdot \left\{ 33.10|_{\text{SM}} + \left(1 + \text{Re } g_{st}^{\text{eff}}\right) \left[r_H \left(-48.93 - 47.60 \log r_H - 0.99 (\log r_H)^2 \right. \right. \right. \\
 \left. \left. - 0.15 (\log r_H)^3 + 4.71 \text{Li}_2 \left(1 - \frac{1}{r_H} \right) \right) \right. \\
 \left. + r_H^2 \left(-53.82 - 98.18 \log r_H + 4.79 \text{Li}_2 \left(1 - \frac{1}{r_H} \right) \right) \right. \\
 \left. + r_H^3 \left(-56.04 - 150.43 \log r_H + 3.17 \text{Li}_2 \left(1 - \frac{1}{r_H} \right) \right) \right] \right\}, \tag{7.5}
 \end{aligned}$$

which agrees with the exact result within 1% in the complete subdomain of $(M_{H^\pm}, \text{Re } g_{st}^{\text{eff}}) \in [500 \text{ GeV}, \infty) \times [-5, 5]$ in which R_γ lies within the band allowed by the experimental and theoretical uncertainties (see below). The approximate formula in eq. (7.5) only includes the interference of the new-physics contribution with the SM result and neglects the squared new-physics contribution. In deriving eq. (7.5) we have used eq. (10) of ref. [102]. We adopt the estimate of the theoretical uncertainty of about 6.73% given in [25], consisting of individual uncertainties of 5% (non-perturbative), 1.5% (parametric), 3% (higher-order), and 3% (interpolation in the charm quark mass m_c). In figure 8, we illustrate the ratio R_γ in the $(M_{H^\pm}, \text{Re } g_{st}^{\text{eff}})$ plane. The thick dashed line corresponds to the central experimental value in eq. (7.2) and $R_{\gamma, \text{exp}} \pm \Delta_{\text{exp+th}}$, where $\Delta_{\text{exp+th}} = 2\sigma_{\text{exp}} + \delta_{\text{th}}$ is the sum of the experimental 2σ uncertainty intervals and the theoretical uncertainty of 6.73%. For small values of M_{H^\pm} , the allowed range of g_{st}^{eff} is tightly constrained around $g_{st}^{\text{eff}} = -1$, due to the closeness of the Standard Model prediction and the experimental central value. At larger M_{H^\pm} , a significantly wider range of flavour-changing Yukawa couplings is allowed. From R_γ we derive M_{H^\pm} -dependent upper and lower bounds on $\text{Re}(g_{st}^{\text{eff}})$ which we will use in order to constrain the real part of the flavour-changing up-type couplings appearing in $B_s \rightarrow \mu^+ \mu^-$.

7.2 Higgs searches

Searches for heavy Higgs bosons at the LHC put powerful lower limits on the masses of new Higgs particles, but these depend on the Yukawa sector of the considered 2HDM. For the case of the type-II model (or ramifications of it) these searches already exclude a significant portion of the $M_{A^0} - \tan\beta$ plane at present. In figure 9, we show a recent collection of exclusion limits obtained through various different searches by the ATLAS experiment [95] in

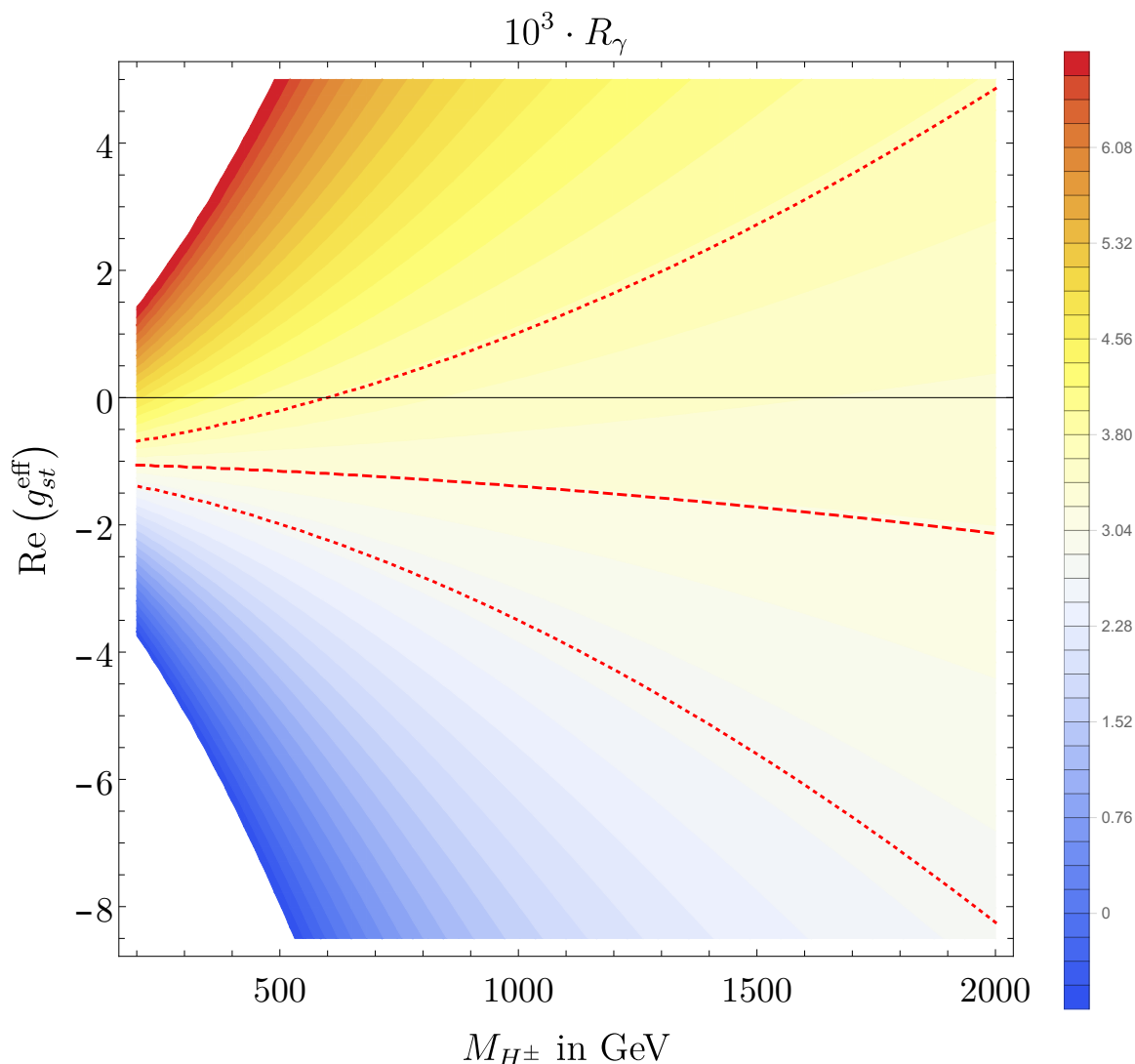


Figure 8. The ratio R_γ as a function of the charged Higgs boson mass M_{H^\pm} and g_{st}^{eff} . The dashed lines correspond to the experimental central value and the $\pm 2\sigma$ intervals, to which we have also added the theoretical uncertainties.

a modification of the type-II model. These limits imply that large values of $\tan\beta$ can only be realised if at the same time the additional Higgs bosons are quite heavy, $M_{A^0} \gtrsim 1.5$ TeV.

It should be noted that for heavy M_{A^0} these bounds also approximately apply for M_{H^+} and M_{H^0} , since the masses become degenerate in the heavy-Higgs limit (for a thorough analysis of the allowed mass splittings see [71]; see also the vertical dashed lines in figure 3). Note that the bounds from neutral Higgs searches are more constraining than those for H^+ searches [94]. The most stringent constraints are from final states with τ 's and also apply to our lepton Yukawa Lagrangian in eq. (2.21) which we have chosen of type-II. (However, the choice of the τ Yukawa couplings is of no relevance for the phenomenology of the $b \rightarrow s$ FCNC processes discussed in this paper.) The presence of the additional couplings g_{jk}^u will increase some branching ratios at the expense of those of decays into τ 's, so that these bounds

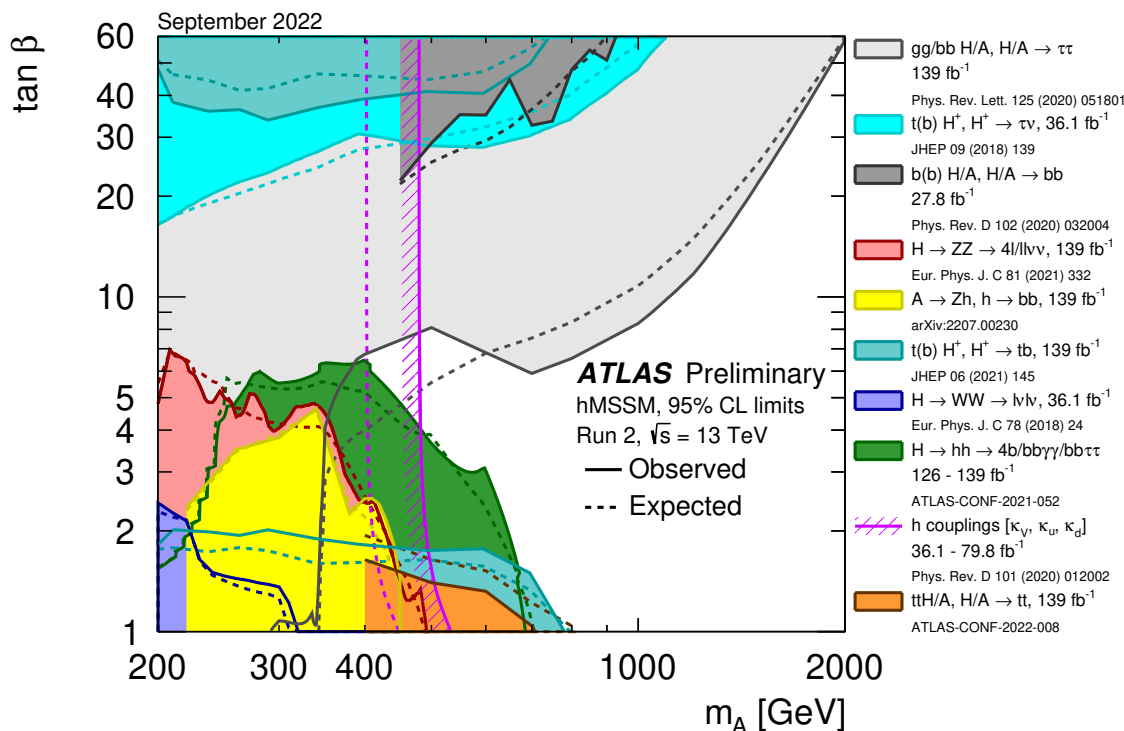


Figure 9. Exclusion limits in the $M_{A^0} - \tan \beta$ plane from different searches performed by the ATLAS experiment; the plot is taken from ref. [95]. The shown limits are for a different variant of the type-II 2HDM than ours, but qualitatively apply as well to our model.

can be somewhat weakened, but the general trend remains valid. Our scenarios discussed below comply with the ATLAS bounds.

7.3 $B_s - \bar{B}_s$ mixing

The effective $\bar{s}_L b_R A^0$ and $\bar{s}_L b_R H^0$ vertices are the sum of the tree-level couplings $\propto g_{sb}$ and the loop contributions involving vertex and self-energy diagrams $\propto g_{ut} V_{tb} V_{us}^* + g_{ct} V_{tb} V_{cs}^* + g_{tt} V_{tb} V_{ts}^*$. The coefficients C_P and C_S are proportional to this effective vertex, which is therefore the relevant quantity constrained by $\mathcal{B}(B_s \rightarrow \mu^+ \mu^-)$. Now the $B_s - \bar{B}_s$ mixing amplitude depends quadratically on this effective vertex, while both quantities decrease quadratically with M_{A^0} and M_{H^0} , so that the quantities give complementary information on the parameter space. $B_s - \bar{B}_s$ mixing is mediated in the Standard Model by the $|\Delta B| = 2$ operator $Q_{VLL} = (\bar{b}_L \gamma_\mu s_L) (\bar{b}_L \gamma^\mu s_L)$ and in the 2HDM by three additional effective operators

$$\begin{aligned}
 Q_{SLL} &= (\bar{b}_{RSL}) (\bar{b}_{RSL}) , \\
 Q_{SLR} &= (\bar{b}_{RSL}) (\bar{b}_{LSR}) , \\
 Q_{SRR} &= (\bar{b}_{LSR}) (\bar{b}_{LSR}) ,
 \end{aligned}
 \tag{7.6}$$

The Wilson coefficient of Q_{SLL} only involves the effective vertex governing $B_s \rightarrow \mu^+ \mu^-$ and the tree-level propagators of A^0 and H^0 , while the coefficients of the other operators also involve

the corresponding chirality-flipped effective $\bar{s}_R b_L A^0$ and $\bar{s}_R b_L H^0$ vertices. The coefficient C_{SLL} (C_{SRR}) is proportional to m_b^2 (m_s^2), while the coefficient C_{SLR} is proportional to $m_b m_s$; we therefore drop the operator Q_{SRR} in our analysis. However, considering the ATLAS constraints implying large masses M_{A^0, H^0} , $C_{SLL} \propto 1/M_{A^0}^2 - 1/M_{H^0}^2$ is heavily suppressed due to the small splitting of Higgs masses in the large-mass limit, and C_{SLR} becomes relevant. This feature results from the fact that Q_{SLL} violates hypercharge by two units of the Higgs hypercharge and the coefficient C_{SLL} is therefore suppressed by a factor of $v^2/M_{A^0}^2$ compared to C_{SLR} multiplying Q_{SLR} which conserves hypercharge and SU(2). As a consequence, C_{SLR} is more important than C_{SLL} . This feature has been widely studied in the context of the effective 2HDM emerging from integrating out superpartners in the MSSM [33–35, 37].

In the following we correlate $\mathcal{B}(B_s \rightarrow \mu^+ \mu^-)$ with $\mathcal{B}(B \rightarrow X_s \gamma)$ and the $B_s - \bar{B}_s$ oscillation frequency ΔM_{B_s} , which is proportional to the magnitude of the $B_s - \bar{B}_s$ mixing amplitude. Only the effective $\bar{s}_L b_R A^0$ and $\bar{s}_L b_R H^0$ vertices are physical, by e.g. changing the renormalisation condition for g_{sb} we can shift pieces between g_{sb} and the renormalised loop. For simplicity, we set the tree-value of g_{sb} to zero, i.e. consider the case that this coupling is only generated radiatively. The only non-trivial Yukawa structure entering the considered observables is then g_{st}^{eff} .

In figure 10 and figure 11 we illustrate the dependence of the branching ratio $\mathcal{B}(B_s \rightarrow \mu^+ \mu^-)$ on the flavour-changing Yukawa couplings for some exemplary numerical values. We choose to show our results separately for the LHCb [68, 69] and CMS [70] measurements, which lie on different sides of the SM prediction calculated with the value $|V_{cb}|$ taken from inclusive decays. The interval allowed on the horizontal axis (the real part $\text{Re}(g_{st}^{\text{eff}})$) is for each choice of Higgs masses determined by the range allowed by $b \rightarrow s \gamma$. Recall that g_{st}^{eff} carries a factor of $\tan \beta$, which needs to be taken into account if the bounds on g_{st}^{eff} were to be converted into direct bounds on g_{ct} . A priori generic $\leq \mathcal{O}(0.1)$ values of g_{ct} could make g_{st}^{eff} in eq. (7.4) as large as $\mathcal{O}(50)$. For the considered Higgs masses such large values of $|g_{st}^{\text{eff}}|$ are forbidden by $b \rightarrow s \gamma$ and the range for $\text{Im}(g_{\text{eff}, bs\gamma})$ shown on the y axis in plots (a) to (d) only serves the purpose to show the constraint from $\mathcal{B}(B_s \rightarrow \mu^+ \mu^-)$. Low values for Higgs masses enforce small values for $\tan \beta$ from the LHC searches, but for these scenarios $b \rightarrow s \gamma$ forbids any measurable effect in $\mathcal{B}(B_s \rightarrow \mu^+ \mu^-)$. This situation changes if one considers large values for $\tan \beta$ and the Higgs masses, because $\mathcal{B}(B_s \rightarrow \mu^+ \mu^-)$ grows faster with $\tan \beta$ than $\mathcal{B}(B \rightarrow X_s \gamma)$, see plots (e) and (f). We find that in the considered scenarios the bounds from $\mathcal{B}(B \rightarrow X_s \gamma)$ are stronger than those from ΔM_{B_s} , which we always find in the band allowed by the current theoretical uncertainty. This situation changes if we go to even larger Higgs masses, permitting larger values of $|g_{st}^{\text{eff}}|$ in $\mathcal{B}(B \rightarrow X_s \gamma)$. The quadratic dependence of ΔM_{B_s} on g_{st}^{eff} makes ΔM_{B_s} a good probe of the parameter region in which both the Higgs masses and g_{st}^{eff} are large.

In order to assess the quality of the perturbative expansions, we discuss the size of the new couplings here. The above-mentioned value $g_{st}^{\text{eff}} \sim 50$ for the product of couplings entering $b \rightarrow s \gamma$ is large, because in eq. (7.4) g_{st}^{eff} is normalised to the type-II result which is suppressed by $\cot \beta$. I.e. in the three-spurion model this suppression is offset, which gives rise to a different phenomenology. Including the prefactor of eq. (7.4) results in the product of couplings of order $0.8|V_{tb}V_{ts}|$ for $g_{st}^{\text{eff}} = 50$, so that even for $g_{st}^{\text{eff}} \gtrsim 50$ perturbation theory is well-behaved and two-loop corrections involving more powers of g_{jt} , $j = u, c, t$ are tiny.

parameter	numerical value	reference
M_{B_s}	5.367 GeV	[103]
m_b	4.18 GeV	[85]
m_s	0.093 GeV	[85]
m_μ	0.106 GeV	[104]
$\bar{m}_t (\bar{m}_t)$	162.622 GeV	[85]
$\alpha_s (M_Z = 91.1876 \text{ GeV})$	0.1179	[85]
G_F	$1.166 \times 10^{-5} \text{ GeV}^{-2}$	[105]
M_W	80.37 GeV	[106]
f_{B_s}	0.230 GeV	[107]
Γ_H^s	$(1.616 \text{ ps})^{-1}$	HFLAV
Γ_L^s	$(1.427 \text{ ps})^{-1}$	HFLAV
$ V_{ts} $	0.041	CKMfitter
$ V_{tb} $	0.999	CKMfitter
$ V_{cs} $	0.974	CKMfitter
$ V_{cb} $	0.041	CKMfitter
$\mathcal{B}(B_s \rightarrow \mu^+ \mu^-)_{\text{SM}}$	$3.65(23) \times 10^{-9}$	[27]
$\mathcal{B}(B_s \rightarrow \mu^+ \mu^-)_{\text{LHCb}}$	$3.09^{+0.48}_{-0.44} \times 10^{-9}$	[68, 69]
$\mathcal{B}(B_s \rightarrow \mu^+ \mu^-)_{\text{CMS}}$	$3.95^{+0.52}_{-0.47} \times 10^{-9}$	[70]

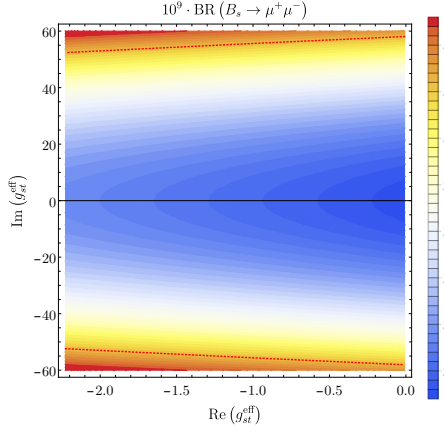
Table 1. Numerical input used for the phenomenological analysis. For the QCD running of the top-quark mass and the renormalisation scale, we have used RunDec [108, 109]. The numerical values of the CKM matrix elements have been taken from the updates provided on the CKMfitter [110] web page. The numerical values of the B_s decay widths have been taken from the online updates provided at the HFLAV web page [86].

We do not study the case of sizable imaginary parts of the new FCNC couplings here. These imaginary parts impact CP asymmetries such as $A_{\text{CP}}^{\text{mix}}(B_s \rightarrow J/\psi\phi)$, which will be investigated in a follow-up paper. All numerical SM input parameters are given in table 1. Note that we do not take into account uncertainties in the input parameters as the dependence of the branching ratio is much weaker than the dependence due to the variation of flavour-changing Yukawa couplings.

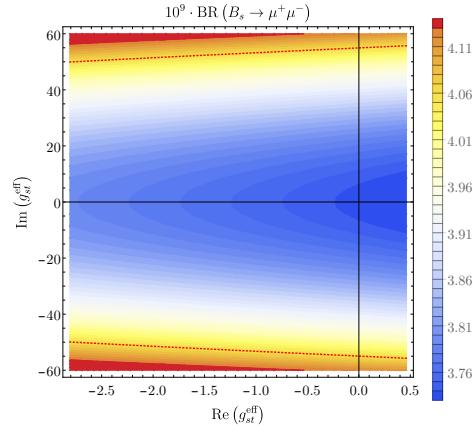
We stress here that the presented calculation equally applies to $B_d \rightarrow \mu^+ \mu^-$ with the change $V_{ts} \rightarrow V_{td}$, but this is not true anymore when considering the constraint from $B_d - \bar{B}_d$ mixing because of the additional dependence on the light quark mass. Since m_d is negligibly small, the $B_d - \bar{B}_d$ mixing amplitude becomes insensitive to the effective $\bar{b}dA^0$ and $\bar{b}dH^0$ couplings in the limit of large and degenerate Higgs-boson masses.

8 Summary

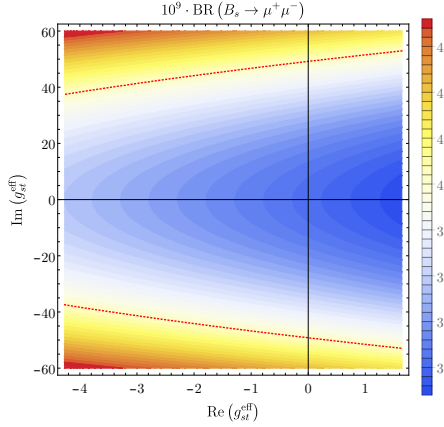
We have presented a 2HDM with three flavour-breaking spurions in the quark Yukawa sector. The model contains the established type-I and type-II models as limiting cases and otherwise permits large FCNC couplings in the up-type sector while naturally suppressing FCNC effects



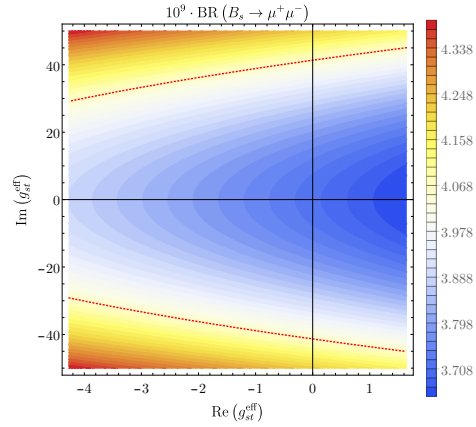
(a) $M_{H^\pm} = M_{H^0} = M_{A^0} = 600 \text{ GeV}$, $\tan \beta = 7$.



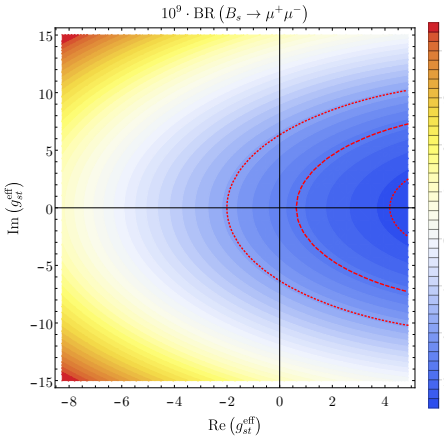
(b) $M_{H^\pm} = M_{A^0} = 800 \text{ GeV}$, $M_{H^0} = 600 \text{ GeV}$, $\tan \beta = 7$.



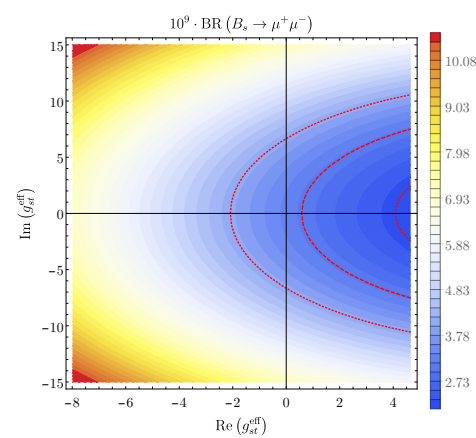
(c) $M_{H^\pm} = M_{H^0} = M_{A^0} = 1200 \text{ GeV}$, $\tan \beta = 12$.



(d) $M_{H^\pm} = 1200 \text{ GeV}$, $M_{H^0} = M_{A^0} = 1100 \text{ GeV}$, $\tan \beta = 12$.

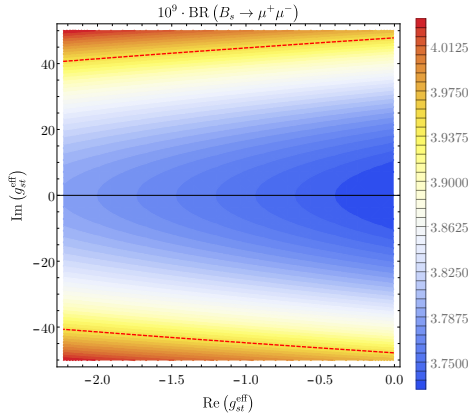


(e) $M_{H^\pm} = M_{H^0} = M_{A^0} = 2000 \text{ GeV}$, $\tan \beta = 60$.

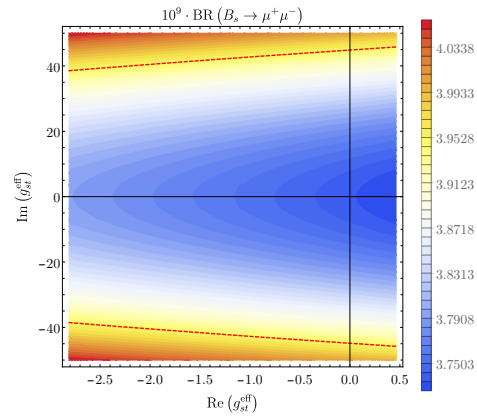


(f) $M_{H^\pm} = 1950 \text{ GeV}$, $M_{H^0} = 2050 \text{ GeV}$, $M_{A^0} = 2000 \text{ GeV}$, $\tan \beta = 60$.

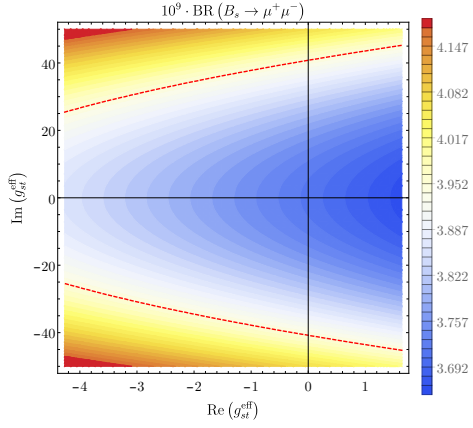
Figure 10. Branching ratio of $B_s \rightarrow \mu^+ \mu^-$ for different values of Higgs masses and $\tan \beta$. All quantities are evaluated at $\mu = \bar{m}_t$ (\bar{m}_t). The red dashed and dotted lines indicate the experimental central value and the 2σ uncertainties of LHCb branching ratio measurement [68, 69], respectively. The constraint of $\mathcal{B}(B \rightarrow X_s \gamma)$ on $|\text{Im } g_{st}^{\text{eff}}|$ is not shown.



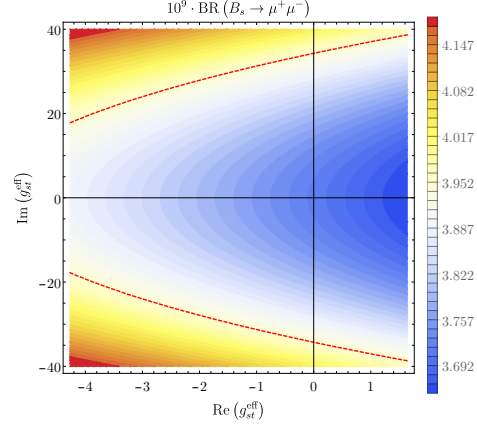
(a) $M_{H^\pm} = M_{H^0} = M_{A^0} = 600 \text{ GeV}$, $\tan \beta = 7$.



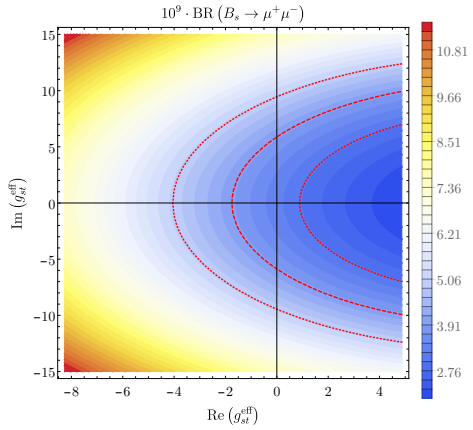
(b) $M_{H^\pm} = M_{A^0} = 800 \text{ GeV}$, $M_{H^0} = 600 \text{ GeV}$, $\tan \beta = 7$.



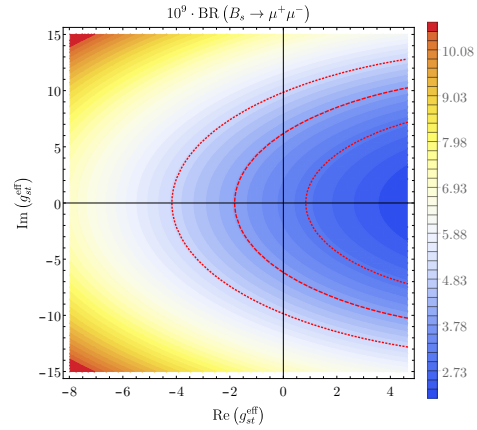
(c) $M_{H^\pm} = M_{H^0} = M_{A^0} = 1200 \text{ GeV}$, $\tan \beta = 12$.



(d) $M_{H^\pm} = 1200 \text{ GeV}$, $M_{H^0} = M_{A^0} = 1100 \text{ GeV}$, $\tan \beta = 12$.



(e) $M_{H^\pm} = M_{H^0} = M_{A^0} = 2000 \text{ GeV}$, $\tan \beta = 60$.



(f) $M_{H^\pm} = 1950 \text{ GeV}$, $M_{H^0} = 2050 \text{ GeV}$, $M_{A^0} = 2000 \text{ GeV}$, $\tan \beta = 60$.

Figure 11. Same as figure 10 for the CMS branching ratio measurement [70].

in down sector, as required by data. Despite the large number of parameters the model makes characteristic predictions, such as correlations between $b \rightarrow s\mu^+\mu^-$, $b \rightarrow s\gamma$, and $B_s - \bar{B}_s$ mixing, all of which involve the same combination g_{st}^{eff} of fundamental parameters. Also all couplings to right-handed down-type quarks are proportional to the quark masses as in the type-II model.

We have studied in detail the rare decay $B_s \rightarrow \mu^+\mu^-$, calculated the Wilson coefficients of the effective operators Q_S and Q_P , and demonstrated the consistency of the model by showing that the UV counterterms follow the pattern of the spurion expansion. Next we have calculated next-to-leading order (two-loop) QCD corrections to this process to (i) verify that higher-order QCD corrections can be correctly included (e.g. all UV divergences could be renormalised in the usual way plus counterterms for our new couplings) and (ii) tame the sizable renormalisation-scale dependence of the Yukawa couplings. Then we have studied the phenomenology of an FCNC coupling g_{ct} of the heavy neutral Higgs bosons to top and charm quarks. We have found that — contrary to expectation — the dominant contribution to the loop-induced $\bar{s}_L b_R A^0$ and $\bar{s}_L b_R H^0$ couplings do not come from vertex diagrams with the neutral Higgs coupling to the internal top-charm line, but from charged-Higgs couplings which inherit the dependence on g_{ct} through SU(2) symmetry. The corresponding diagram (FCNC self-energy with the neutral Higgs attached to the b line) is enhanced by a factor of $\tan\beta$ compared to the vertex diagram, resulting in a $\mathcal{O}(\tan^3\beta)$ contribution to the $B_s \rightarrow \mu^+\mu^-$ amplitude which is absent in the type-II model. This feature makes $B_s \rightarrow \mu^+\mu^-$ a sensitive probe of the model even for Higgs masses well above the lower bounds found by the LHC experiments. For small Higgs masses, however, $b \rightarrow s\gamma$ precludes large effects in $B_s \rightarrow \mu^+\mu^-$. In our model the dominant contribution to $B_s - \bar{B}_s$ mixing is naturally small due to a suppression factor of $m_s m_b / v^2$; nevertheless $B_s - \bar{B}_s$ mixing sets constraints on the parameter space for very large Higgs masses.

Acknowledgments

M.S.L. would like to thank Florian Herren, Syuhei Iguro, Lucas Kunz and Mustafa Tabet for helpful discussions. The authors are grateful to Matthias Steinhauser for collaboration in an early stage of the project. This research was supported by the BMBF grants 05H18VKCC1 and 05H21VKKBA as well as Deutsche Forschungsgemeinschaft (DFG, German Research Foundation) within the Collaborative Research Center *Particle Physics Phenomenology after the Higgs Discovery (P3H)* (project no. 396021762 — TRR 257). All Feynman diagrams within this paper have been produced using TikZ-FeynHand [111, 112].

Open Access. This article is distributed under the terms of the Creative Commons Attribution License ([CC-BY4.0](https://creativecommons.org/licenses/by/4.0/)), which permits any use, distribution and reproduction in any medium, provided the original author(s) and source are credited.

References

- [1] G.C. Branco et al., *Theory and phenomenology of two-Higgs-doublet models*, *Phys. Rept.* **516** (2012) 1 [[arXiv:1106.0034](https://arxiv.org/abs/1106.0034)] [[INSPIRE](https://inspirehep.net/literature/1000000)].
- [2] J.F. Gunion, H.E. Haber, G. Kane and D. Sally, *The Higgs Hunter's Guide*, CRC Press (2018) [[DOI:10.1201/9780429496448](https://doi.org/10.1201/9780429496448)].

- [3] J.E. Kim, *Light Pseudoscalars, Particle Physics and Cosmology*, *Phys. Rept.* **150** (1987) 1 [INSPIRE].
- [4] R.D. Peccei and H.R. Quinn, *CP Conservation in the Presence of Instantons*, *Phys. Rev. Lett.* **38** (1977) 1440 [INSPIRE].
- [5] R.D. Peccei and H.R. Quinn, *Constraints Imposed by CP Conservation in the Presence of Instantons*, *Phys. Rev. D* **16** (1977) 1791 [INSPIRE].
- [6] H.E. Haber and G.L. Kane, *The Search for Supersymmetry: Probing Physics Beyond the Standard Model*, *Phys. Rept.* **117** (1985) 75 [INSPIRE].
- [7] A. Crivellin, C. Greub and A. Kokulu, *Explaining $B \rightarrow D\tau\nu$, $B \rightarrow D^*\tau\nu$ and $B \rightarrow \tau\nu$ in a 2HDM of type III*, *Phys. Rev. D* **86** (2012) 054014 [arXiv:1206.2634] [INSPIRE].
- [8] A. Crivellin, A. Kokulu and C. Greub, *Flavor-phenomenology of two-Higgs-doublet models with generic Yukawa structure*, *Phys. Rev. D* **87** (2013) 094031 [arXiv:1303.5877] [INSPIRE].
- [9] A. Crivellin, D. Müller and C. Wiegand, *$b \rightarrow s\ell^+\ell^-$ transitions in two-Higgs-doublet models*, *JHEP* **06** (2019) 119 [arXiv:1903.10440] [INSPIRE].
- [10] HFLAV collaboration, *Averages of b -hadron, c -hadron, and τ -lepton properties as of 2021*, *Phys. Rev. D* **107** (2023) 052008 [arXiv:2206.07501] [INSPIRE].
- [11] BABAR collaboration, *Evidence for an excess of $\bar{B} \rightarrow D^{(*)}\tau^-\bar{\nu}_\tau$ decays*, *Phys. Rev. Lett.* **109** (2012) 101802 [arXiv:1205.5442] [INSPIRE].
- [12] BABAR collaboration, *Measurement of an Excess of $\bar{B} \rightarrow D^{(*)}\tau^-\bar{\nu}_\tau$ Decays and Implications for Charged Higgs Bosons*, *Phys. Rev. D* **88** (2013) 072012 [arXiv:1303.0571] [INSPIRE].
- [13] BELLE collaboration, *Measurement of the branching ratio of $\bar{B} \rightarrow D^{(*)}\tau^-\bar{\nu}_\tau$ relative to $\bar{B} \rightarrow D^{(*)}\ell^-\bar{\nu}_\ell$ decays with hadronic tagging at Belle*, *Phys. Rev. D* **92** (2015) 072014 [arXiv:1507.03233] [INSPIRE].
- [14] LHCb collaboration, *Measurement of the ratio of branching fractions $\mathcal{B}(\bar{B}^0 \rightarrow D^{*+}\tau^-\bar{\nu}_\tau)/\mathcal{B}(\bar{B}^0 \rightarrow D^{*+}\mu^-\bar{\nu}_\mu)$* , *Phys. Rev. Lett.* **115** (2015) 111803 [Erratum *ibid.* **115** (2015) 159901] [arXiv:1506.08614] [INSPIRE].
- [15] BELLE collaboration, *Measurement of the τ lepton polarization and $R(D^*)$ in the decay $\bar{B} \rightarrow D^*\tau^-\bar{\nu}_\tau$* , *Phys. Rev. Lett.* **118** (2017) 211801 [arXiv:1612.00529] [INSPIRE].
- [16] BELLE collaboration, *Measurement of the τ lepton polarization and $R(D^*)$ in the decay $\bar{B} \rightarrow D^*\tau^-\bar{\nu}_\tau$ with one-prong hadronic τ decays at Belle*, *Phys. Rev. D* **97** (2018) 012004 [arXiv:1709.00129] [INSPIRE].
- [17] LHCb collaboration, *Measurement of the ratio of the $B^0 \rightarrow D^{*-}\tau^+\nu_\tau$ and $B^0 \rightarrow D^{*-}\mu^+\nu_\mu$ branching fractions using three-prong τ -lepton decays*, *Phys. Rev. Lett.* **120** (2018) 171802 [arXiv:1708.08856] [INSPIRE].
- [18] LHCb collaboration, *Test of Lepton Flavor Universality by the measurement of the $B^0 \rightarrow D^{*-}\tau^+\nu_\tau$ branching fraction using three-prong τ decays*, *Phys. Rev. D* **97** (2018) 072013 [arXiv:1711.02505] [INSPIRE].
- [19] BELLE collaboration, *Measurement of $\mathcal{R}(D)$ and $\mathcal{R}(D^*)$ with a semileptonic tagging method*, *Phys. Rev. Lett.* **124** (2020) 161803 [arXiv:1910.05864] [INSPIRE].
- [20] LHCb collaboration, *Measurement of the ratios of branching fractions $\mathcal{R}(D^*)$ and $\mathcal{R}(D^0)$* , *Phys. Rev. Lett.* **131** (2023) 111802 [arXiv:2302.02886] [INSPIRE].
- [21] LHCb collaboration, *Test of lepton flavor universality using $B^0 \rightarrow D^{*-}\tau^+\nu_\tau$ decays with hadronic τ channels*, *Phys. Rev. D* **108** (2023) 012018 [arXiv:2305.01463] [INSPIRE].

- [22] H.E. Haber and D. O’Neil, *Basis-independent methods for the two-Higgs-doublet model. II. The Significance of $\tan\beta$* , *Phys. Rev. D* **74** (2006) 015018 [Erratum *ibid.* **74** (2006) 059905] [[hep-ph/0602242](#)] [[INSPIRE](#)].
- [23] D. Eriksson, J. Rathsman and O. Stal, *2HDMC: Two-Higgs-Doublet Model Calculator Physics and Manual*, *Comput. Phys. Commun.* **181** (2010) 189 [[arXiv:0902.0851](#)] [[INSPIRE](#)].
- [24] G.C. Branco, L. Lavoura and J.P. Silva, *CP Violation*, Clarendon Press (1999) [[INSPIRE](#)].
- [25] M. Misiak and M. Steinhauser, *Weak radiative decays of the B meson and bounds on M_{H^\pm} in the Two-Higgs-Doublet Model*, *Eur. Phys. J. C* **77** (2017) 201 [[arXiv:1702.04571](#)] [[INSPIRE](#)].
- [26] H.E. Logan and U. Nierste, *$B_{s,d} \rightarrow \ell^+ \ell^-$ in a two Higgs doublet model*, *Nucl. Phys. B* **586** (2000) 39 [[hep-ph/0004139](#)] [[INSPIRE](#)].
- [27] C. Bobeth et al., *$B_{s,d} \rightarrow l^+ l^-$ in the Standard Model with Reduced Theoretical Uncertainty*, *Phys. Rev. Lett.* **112** (2014) 101801 [[arXiv:1311.0903](#)] [[INSPIRE](#)].
- [28] T. Hermann, M. Misiak and M. Steinhauser, *Three-loop QCD corrections to $B_s \rightarrow \mu^+ \mu^-$* , *JHEP* **12** (2013) 097 [[arXiv:1311.1347](#)] [[INSPIRE](#)].
- [29] T. Banks, *Supersymmetry and the Quark Mass Matrix*, *Nucl. Phys. B* **303** (1988) 172 [[INSPIRE](#)].
- [30] L.J. Hall, R. Rattazzi and U. Sarid, *The top quark mass in supersymmetric SO(10) unification*, *Phys. Rev. D* **50** (1994) 7048 [[hep-ph/9306309](#)] [[INSPIRE](#)].
- [31] M. Carena, M. Olechowski, S. Pokorski and C.E.M. Wagner, *Electroweak symmetry breaking and bottom-top Yukawa unification*, *Nucl. Phys. B* **426** (1994) 269 [[hep-ph/9402253](#)] [[INSPIRE](#)].
- [32] K.S. Babu and C.F. Kolda, *Higgs mediated $B^0 \rightarrow \mu^+ \mu^-$ in minimal supersymmetry*, *Phys. Rev. Lett.* **84** (2000) 228 [[hep-ph/9909476](#)] [[INSPIRE](#)].
- [33] G. Isidori and A. Retico, *Scalar flavor changing neutral currents in the large $\tan\beta$ limit*, *JHEP* **11** (2001) 001 [[hep-ph/0110121](#)] [[INSPIRE](#)].
- [34] A.J. Buras, P.H. Chankowski, J. Rosiek and L. Ślawniowska, *$\Delta M_{d,s}, B^0 d, s \rightarrow \mu^+ \mu^-$ and $B \rightarrow X_s \gamma$ in supersymmetry at large $\tan\beta$* , *Nucl. Phys. B* **659** (2003) 3 [[hep-ph/0210145](#)] [[INSPIRE](#)].
- [35] A.J. Buras, P.H. Chankowski, J. Rosiek and L. Ślawniowska, *Correlation between ΔM_s and $B_{s,d}^0 \rightarrow \mu^+ \mu^-$ in supersymmetry at large $\tan\beta$* , *Phys. Lett. B* **546** (2002) 96 [[hep-ph/0207241](#)] [[INSPIRE](#)].
- [36] L. Hofer, U. Nierste and D. Scherer, *Resummation of \tan -beta-enhanced supersymmetric loop corrections beyond the decoupling limit*, *JHEP* **10** (2009) 081 [[arXiv:0907.5408](#)] [[INSPIRE](#)].
- [37] M. Gorbahn, S. Jäger, U. Nierste and S. Trine, *The supersymmetric Higgs sector and $B - \bar{B}$ mixing for large $\tan\beta$* , *Phys. Rev. D* **84** (2011) 034030 [[arXiv:0901.2065](#)] [[INSPIRE](#)].
- [38] A. Dedes, H.K. Dreiner and U. Nierste, *Correlation of $B_s \rightarrow \mu^+ \mu^-$ and $(g - 2)_\mu$ in minimal supergravity*, *Phys. Rev. Lett.* **87** (2001) 251804 [[hep-ph/0108037](#)] [[INSPIRE](#)].
- [39] U. Nierste, M. Tabet and R. Ziegler, *Cornering Spontaneous CP Violation with Charged-Higgs-Boson Searches*, *Phys. Rev. Lett.* **125** (2020) 031801 [[arXiv:1912.11501](#)] [[INSPIRE](#)].
- [40] R.S. Chivukula and H. Georgi, *Composite Technicolor Standard Model*, *Phys. Lett. B* **188** (1987) 99 [[INSPIRE](#)].
- [41] G. D’Ambrosio, G.F. Giudice, G. Isidori and A. Strumia, *Minimal flavor violation: An effective field theory approach*, *Nucl. Phys. B* **645** (2002) 155 [[hep-ph/0207036](#)] [[INSPIRE](#)].

- [42] P. Tuzon and A. Pich, *The Aligned two-Higgs Doublet model*, *Acta Phys. Polon. Supp.* **3** (2010) 215 [[arXiv:1001.0293](#)] [[INSPIRE](#)].
- [43] A. Celis, M. Jung, X.-Q. Li and A. Pich, *Sensitivity to charged scalars in $B \rightarrow D^{(*)}\tau\nu_\tau$ and $B \rightarrow \tau\nu_\tau$ decays*, *JHEP* **01** (2013) 054 [[arXiv:1210.8443](#)] [[INSPIRE](#)].
- [44] O. Eberhardt, A.P. Martínez and A. Pich, *Global fits in the Aligned Two-Higgs-Doublet model*, *JHEP* **05** (2021) 005 [[arXiv:2012.09200](#)] [[INSPIRE](#)].
- [45] C. Bobeth, M. Gorbahn and E. Stamou, *Electroweak Corrections to $B_{s,d} \rightarrow \ell^+\ell^-$* , *Phys. Rev. D* **89** (2014) 034023 [[arXiv:1311.1348](#)] [[INSPIRE](#)].
- [46] K. De Bruyn et al., *Branching Ratio Measurements of B_s Decays*, *Phys. Rev. D* **86** (2012) 014027 [[arXiv:1204.1735](#)] [[INSPIRE](#)].
- [47] K. De Bruyn et al., *Probing New Physics via the $B_s^0 \rightarrow \mu^+\mu^-$ Effective Lifetime*, *Phys. Rev. Lett.* **109** (2012) 041801 [[arXiv:1204.1737](#)] [[INSPIRE](#)].
- [48] N.D. Christensen et al., *A comprehensive approach to new physics simulations*, *Eur. Phys. J. C* **71** (2011) 1541 [[arXiv:0906.2474](#)] [[INSPIRE](#)].
- [49] A. Alloul et al., *FeynRules 2.0 — A complete toolbox for tree-level phenomenology*, *Comput. Phys. Commun.* **185** (2014) 2250 [[arXiv:1310.1921](#)] [[INSPIRE](#)].
- [50] C. Degrande et al., *UFO — The Universal FeynRules Output*, *Comput. Phys. Commun.* **183** (2012) 1201 [[arXiv:1108.2040](#)] [[INSPIRE](#)].
- [51] M. Gerlach, F. Herren and M. Lang, *tapir: A tool for topologies, amplitudes, partial fraction decomposition and input for reductions*, *Comput. Phys. Commun.* **282** (2023) 108544 [[arXiv:2201.05618](#)] [[INSPIRE](#)].
- [52] P. Nogueira, *Automatic Feynman Graph Generation*, *J. Comput. Phys.* **105** (1993) 279 [[INSPIRE](#)].
- [53] B. Ruijl, T. Ueda and J. Vermaseren, *FORM version 4.2*, [arXiv:1707.06453](#) [[INSPIRE](#)].
- [54] R. Harlander, T. Seidensticker and M. Steinhauser, *Complete corrections of $O(\alpha_s)$ to the decay of the Z boson into bottom quarks*, *Phys. Lett. B* **426** (1998) 125 [[hep-ph/9712228](#)] [[INSPIRE](#)].
- [55] T. Seidensticker, *Automatic application of successive asymptotic expansions of Feynman diagrams*, in the proceedings of the *6th International Workshop on New Computing Techniques in Physics Research: Software Engineering, Artificial Intelligence Neural Nets, Genetic Algorithms, Symbolic Algebra, Automatic Calculation*, Heraklion, Greece, April 12–16 (1999) [[hep-ph/9905298](#)] [[INSPIRE](#)].
- [56] A.I. Davydychev and J.B. Tausk, *Two loop selfenergy diagrams with different masses and the momentum expansion*, *Nucl. Phys. B* **397** (1993) 123 [[INSPIRE](#)].
- [57] J.E. Salomon, *Das Laufen und die Vereinigung der Eichkopplungen des Standardmodells zur Drei-Schleifen-Ordnung*, Ph.D. thesis, KIT, Karlsruhe, 76131 Karlsruhe, Germany (2012) [[INSPIRE](#)].
- [58] T. Inami and C.S. Lim, *Effects of Superheavy Quarks and Leptons in Low-Energy Weak Processes $K_L \rightarrow \mu\bar{\mu}$, $K^+ \rightarrow \pi + \nu\bar{\nu}$ and $K^0 \leftrightarrow \bar{K}^0$* , *Prog. Theor. Phys.* **65** (1981) 297 [Erratum *ibid.* **65** (1981) 1772] [[INSPIRE](#)].
- [59] G. Buchalla and A.J. Buras, *QCD corrections to the $\bar{s}dZ$ vertex for arbitrary top quark mass*, *Nucl. Phys. B* **398** (1993) 285 [[INSPIRE](#)].
- [60] G. Buchalla and A.J. Buras, *QCD corrections to rare K and B decays for arbitrary top quark mass*, *Nucl. Phys. B* **400** (1993) 225 [[INSPIRE](#)].

- [61] G. Buchalla and A.J. Buras, *The rare decays $K \rightarrow \pi\nu\bar{\nu}$, $B \rightarrow X\nu\bar{\nu}$ and $B \rightarrow l^+l^-$: An Update*, *Nucl. Phys. B* **548** (1999) 309 [[hep-ph/9901288](#)] [[INSPIRE](#)].
- [62] M. Misiak and J. Urban, *QCD corrections to FCNC decays mediated by Z penguins and W boxes*, *Phys. Lett. B* **451** (1999) 161 [[hep-ph/9901278](#)] [[INSPIRE](#)].
- [63] M. Beneke, C. Bobeth and R. Szafron, *Enhanced electromagnetic correction to the rare B-meson decay $B_{s,d} \rightarrow \mu^+\mu^-$* , *Phys. Rev. Lett.* **120** (2018) 011801 [[arXiv:1708.09152](#)] [[INSPIRE](#)].
- [64] M. Beneke, C. Bobeth and R. Szafron, *Power-enhanced leading-logarithmic QED corrections to $B_q \rightarrow \mu^+\mu^-$* , *JHEP* **10** (2019) 232 [*Erratum ibid.* **11** (2022) 099] [[arXiv:1908.07011](#)] [[INSPIRE](#)].
- [65] C. Bobeth, T. Ewerth, F. Krüger and J. Urban, *Analysis of neutral Higgs boson contributions to the decays $\bar{B}(s) \rightarrow \ell^+\ell^-$ and $\bar{B} \rightarrow K\ell^+\ell^-$* , *Phys. Rev. D* **64** (2001) 074014 [[hep-ph/0104284](#)] [[INSPIRE](#)].
- [66] C. Bobeth, A.J. Buras, F. Krüger and J. Urban, *QCD corrections to $\bar{B} \rightarrow X_{d,s}\nu\bar{\nu}$, $\bar{B}_{d,s} \rightarrow \ell^+\ell^-$, $K \rightarrow \pi\nu\bar{\nu}$ and $K_L \rightarrow \mu^+\mu^-$ in the MSSM*, *Nucl. Phys. B* **630** (2002) 87 [[hep-ph/0112305](#)] [[INSPIRE](#)].
- [67] T. Hermann, *Seltene B-Meson-Zerfälle innerhalb und jenseits des Standardmodells*, Ph.D. thesis, KIT, Karlsruhe, 76131 Karlsruhe, Germany (2014) [[INSPIRE](#)].
- [68] LHCb collaboration, *Analysis of Neutral B-Meson Decays into Two Muons*, *Phys. Rev. Lett.* **128** (2022) 041801 [[arXiv:2108.09284](#)] [[INSPIRE](#)].
- [69] LHCb collaboration, *Measurement of the $B_s^0 \rightarrow \mu^+\mu^-$ decay properties and search for the $B^0 \rightarrow \mu^+\mu^-$ and $B_s^0 \rightarrow \mu^+\mu^-\gamma$ decays*, *Phys. Rev. D* **105** (2022) 012010 [[arXiv:2108.09283](#)] [[INSPIRE](#)].
- [70] CMS collaboration, *Measurement of $B_s^0 \rightarrow \mu^+\mu^-$ decay properties and search for the $B^0 \rightarrow \mu\mu$ decay in proton-proton collisions at $\sqrt{s} = 13$ TeV*, [CMS-PAS-BPH-21-006](#), CERN, Geneva (2022).
- [71] V. Cacchio, D. Chowdhury, O. Eberhardt and C.W. Murphy, *Next-to-leading order unitarity fits in Two-Higgs-Doublet models with soft \mathbb{Z}_2 breaking*, *JHEP* **11** (2016) 026 [[arXiv:1609.01290](#)] [[INSPIRE](#)].
- [72] D. Chowdhury and O. Eberhardt, *Global fits of the two-loop renormalized Two-Higgs-Doublet model with soft \mathbb{Z}_2 breaking*, *JHEP* **11** (2015) 052 [[arXiv:1503.08216](#)] [[INSPIRE](#)].
- [73] R. Casalbuoni, D. Dominici, R. Gatto and C. Giunti, *Strong Interacting Two Doublet and Doublet Singlet Higgs Models*, *Phys. Lett. B* **178** (1986) 235 [[INSPIRE](#)].
- [74] J. Maalampi, J. Sirkka and I. Vilja, *Tree level unitarity and triviality bounds for two Higgs models*, *Phys. Lett. B* **265** (1991) 371 [[INSPIRE](#)].
- [75] S. Kanemura, T. Kubota and E. Takasugi, *Lee-Quigg-Thacker bounds for Higgs boson masses in a two doublet model*, *Phys. Lett. B* **313** (1993) 155 [[hep-ph/9303263](#)] [[INSPIRE](#)].
- [76] A.G. Akeroyd, A. Arhrib and E.-M. Naimi, *Note on tree level unitarity in the general two Higgs doublet model*, *Phys. Lett. B* **490** (2000) 119 [[hep-ph/0006035](#)] [[INSPIRE](#)].
- [77] I.F. Ginzburg and I.P. Ivanov, *Tree-level unitarity constraints in the most general 2HDM*, *Phys. Rev. D* **72** (2005) 115010 [[hep-ph/0508020](#)] [[INSPIRE](#)].
- [78] J. Horejsi and M. Kladiva, *Tree-unitarity bounds for THDM Higgs masses revisited*, *Eur. Phys. J. C* **46** (2006) 81 [[hep-ph/0510154](#)] [[INSPIRE](#)].

- [79] H.E. Haber and D. O’Neil, *Basis-independent methods for the two-Higgs-doublet model III: The CP-conserving limit, custodial symmetry, and the oblique parameters S, T, U*, *Phys. Rev. D* **83** (2011) 055017 [[arXiv:1011.6188](#)] [[INSPIRE](#)].
- [80] B. Grinstein, C.W. Murphy and P. Uttayarat, *One-loop corrections to the perturbative unitarity bounds in the CP-conserving two-Higgs doublet model with a softly broken \mathbb{Z}_2 symmetry*, *JHEP* **06** (2016) 070 [[arXiv:1512.04567](#)] [[INSPIRE](#)].
- [81] L. Durand, J.M. Johnson and J.L. Lopez, *Perturbative unitarity and high-energy W_L^\pm , Z_L , H scattering. One loop corrections and the Higgs boson coupling*, *Phys. Rev. D* **45** (1992) 3112 [[INSPIRE](#)].
- [82] P.N. Maher, L. Durand and K. Riesselmann, *Two loop renormalization constants and high-energy $2 \rightarrow 2$ scattering amplitudes in the Higgs sector of the Standard Model*, *Phys. Rev. D* **48** (1993) 1061 [*Erratum ibid.* **52** (1995) 553] [[hep-ph/9303233](#)] [[INSPIRE](#)].
- [83] L. Durand, P.N. Maher and K. Riesselmann, *Two loop unitarity constraints on the Higgs boson coupling*, *Phys. Rev. D* **48** (1993) 1084 [[hep-ph/9303234](#)] [[INSPIRE](#)].
- [84] U. Nierste and K. Riesselmann, *Higgs sector renormalization group in the \overline{MS} and \overline{OMS} scheme: The breakdown of perturbation theory for a heavy Higgs*, *Phys. Rev. D* **53** (1996) 6638 [[hep-ph/9511407](#)] [[INSPIRE](#)].
- [85] PARTICLE DATA GROUP collaboration, *Review of Particle Physics*, *PTEP* **2020** (2020) 083C01 [[INSPIRE](#)].
- [86] HFLAV collaboration, *Averages of b-hadron, c-hadron, and τ -lepton properties as of 2018*, *Eur. Phys. J. C* **81** (2021) 226 [[arXiv:1909.12524](#)] [[INSPIRE](#)].
- [87] S. Iguro, *Revival of H^- interpretation of $R_D^{(*)}$ anomaly and closing low mass window*, *Phys. Rev. D* **105** (2022) 095011 [[arXiv:2201.06565](#)] [[INSPIRE](#)].
- [88] M. Blanke, S. Iguro and H. Zhang, *Towards ruling out the charged Higgs interpretation of the $R_{D^{(*)}}$ anomaly*, *JHEP* **06** (2022) 043 [[arXiv:2202.10468](#)] [[INSPIRE](#)].
- [89] M. Blanke et al., *Impact of polarization observables and $B_c \rightarrow \tau\nu$ on new physics explanations of the $b \rightarrow c\tau\nu$ anomaly*, *Phys. Rev. D* **99** (2019) 075006 [[arXiv:1811.09603](#)] [[INSPIRE](#)].
- [90] M. Blanke et al., *Addendum to “Impact of polarization observables and $B_c \rightarrow \tau\nu$ on new physics explanations of the $b \rightarrow c\tau\nu$ anomaly”*, [arXiv:1905.08253](#) [[DOI:10.1103/PhysRevD.100.035035](#)] [[INSPIRE](#)].
- [91] LHCb collaboration, *First joint measurement of $R(D^*)$ and $R(D^0)$ at LHCb*, <https://indico.cern.ch/event/1187939/>.
- [92] S. Iguro, T. Kitahara and R. Watanabe, *Global fit to $b \rightarrow c\tau\nu$ anomalies 2022 mid-autumn*, [arXiv:2210.10751](#) [[INSPIRE](#)].
- [93] M. Fedele et al., *Impact of $\Lambda_b \rightarrow \Lambda_c\tau\nu$ measurement on New Physics in $b \rightarrow c\ell\nu$ transitions*, *Phys. Rev. D* **107** (2023) 055005 [[arXiv:2211.14172](#)] [[INSPIRE](#)].
- [94] ATLAS collaboration, *Search for charged Higgs bosons decaying via $H^\pm \rightarrow \tau^\pm\nu_\tau$ in the τ +jets and τ +lepton final states with 36 fb^{-1} of pp collision data recorded at $\sqrt{s} = 13\text{ TeV}$ with the ATLAS experiment*, *JHEP* **09** (2018) 139 [[arXiv:1807.07915](#)] [[INSPIRE](#)].
- [95] ATLAS collaboration, *Summary plots for beyond Standard Model Higgs boson benchmarks for direct and indirect searches*, [ATL-PHYS-PUB-2022-043](#), CERN, Geneva (2022).

- [96] ATLAS collaboration, *Combined measurements of Higgs boson production and decay using up to 80 fb^{-1} of proton-proton collision data at $\sqrt{s} = 13\text{ TeV}$ collected with the ATLAS experiment*, *Phys. Rev. D* **101** (2020) 012002 [[arXiv:1909.02845](#)] [[INSPIRE](#)].
- [97] CMS collaboration, *Combined measurements of Higgs boson couplings in proton-proton collisions at $\sqrt{s} = 13\text{ TeV}$* , *Eur. Phys. J. C* **79** (2019) 421 [[arXiv:1809.10733](#)] [[INSPIRE](#)].
- [98] M. Jung, A. Pich and P. Tuzon, *Charged-Higgs phenomenology in the Aligned two-Higgs-doublet model*, *JHEP* **11** (2010) 003 [[arXiv:1006.0470](#)] [[INSPIRE](#)].
- [99] M. Jung, A. Pich and P. Tuzon, *The $B \rightarrow X_s \gamma$ Rate and CP Asymmetry within the Aligned Two-Higgs-Doublet Model*, *Phys. Rev. D* **83** (2011) 074011 [[arXiv:1011.5154](#)] [[INSPIRE](#)].
- [100] M. Jung, X.-Q. Li and A. Pich, *Exclusive radiative B-meson decays within the aligned two-Higgs-doublet model*, *JHEP* **10** (2012) 063 [[arXiv:1208.1251](#)] [[INSPIRE](#)].
- [101] T. Hermann, M. Misiak and M. Steinhauser, *$\bar{B} \rightarrow X_s \gamma$ in the Two Higgs Doublet Model up to Next-to-Next-to-Leading Order in QCD*, *JHEP* **11** (2012) 036 [[arXiv:1208.2788](#)] [[INSPIRE](#)].
- [102] M. Misiak et al., *Updated NNLO QCD predictions for the weak radiative B-meson decays*, *Phys. Rev. Lett.* **114** (2015) 221801 [[arXiv:1503.01789](#)] [[INSPIRE](#)].
- [103] LHCb collaboration, *Observation of $B_{(s)}^0 \rightarrow J/\psi p \bar{p}$ decays and precision measurements of the $B_{(s)}^0$ masses*, *Phys. Rev. Lett.* **122** (2019) 191804 [[arXiv:1902.05588](#)] [[INSPIRE](#)].
- [104] P.J. Mohr, D.B. Newell and B.N. Taylor, *CODATA Recommended Values of the Fundamental Physical Constants: 2014*, *Rev. Mod. Phys.* **88** (2016) 035009 [[arXiv:1507.07956](#)] [[INSPIRE](#)].
- [105] MŪLAN collaboration, *Measurement of the Positive Muon Lifetime and Determination of the Fermi Constant to Part-per-Million Precision*, *Phys. Rev. Lett.* **106** (2011) 041803 [[arXiv:1010.0991](#)] [[INSPIRE](#)].
- [106] ATLAS collaboration, *Measurement of the W-boson mass in pp collisions at $\sqrt{s} = 7\text{ TeV}$ with the ATLAS detector*, *Eur. Phys. J. C* **78** (2018) 110 [Erratum *ibid.* **78** (2018) 898] [[arXiv:1701.07240](#)] [[INSPIRE](#)].
- [107] FLAVOUR LATTICE AVERAGING GROUP (FLAG) collaboration, *FLAG Review 2021*, *Eur. Phys. J. C* **82** (2022) 869 [[arXiv:2111.09849](#)] [[INSPIRE](#)].
- [108] K.G. Chetyrkin, J.H. Kühn and M. Steinhauser, *RunDec: A Mathematica package for running and decoupling of the strong coupling and quark masses*, *Comput. Phys. Commun.* **133** (2000) 43 [[hep-ph/0004189](#)] [[INSPIRE](#)].
- [109] F. Herren and M. Steinhauser, *Version 3 of RunDec and CRunDec*, *Comput. Phys. Commun.* **224** (2018) 333 [[arXiv:1703.03751](#)] [[INSPIRE](#)].
- [110] CKMFITTER GROUP collaboration, *CP violation and the CKM matrix: Assessing the impact of the asymmetric B factories*, *Eur. Phys. J. C* **41** (2005) 1 [[hep-ph/0406184](#)] [[INSPIRE](#)].
- [111] M. Dohse, *TikZ-FeynHand: Basic User Guide*, [arXiv:1802.00689](#) [[INSPIRE](#)].
- [112] J. Ellis, *TikZ-Feynman: Feynman diagrams with TikZ*, *Comput. Phys. Commun.* **210** (2017) 103 [[arXiv:1601.05437](#)] [[INSPIRE](#)].